UiT
THE ARCTIC
UNIVERSITY
OF NORWAY

Faculty of Science and Technology
Department of Physics and Technology

Angle Dependent Reflectance and Performance of Solar Cells and Absorbers

Øystein Jordheim

FYS-3900 Master Thesis in Physics 60SP, May 2018

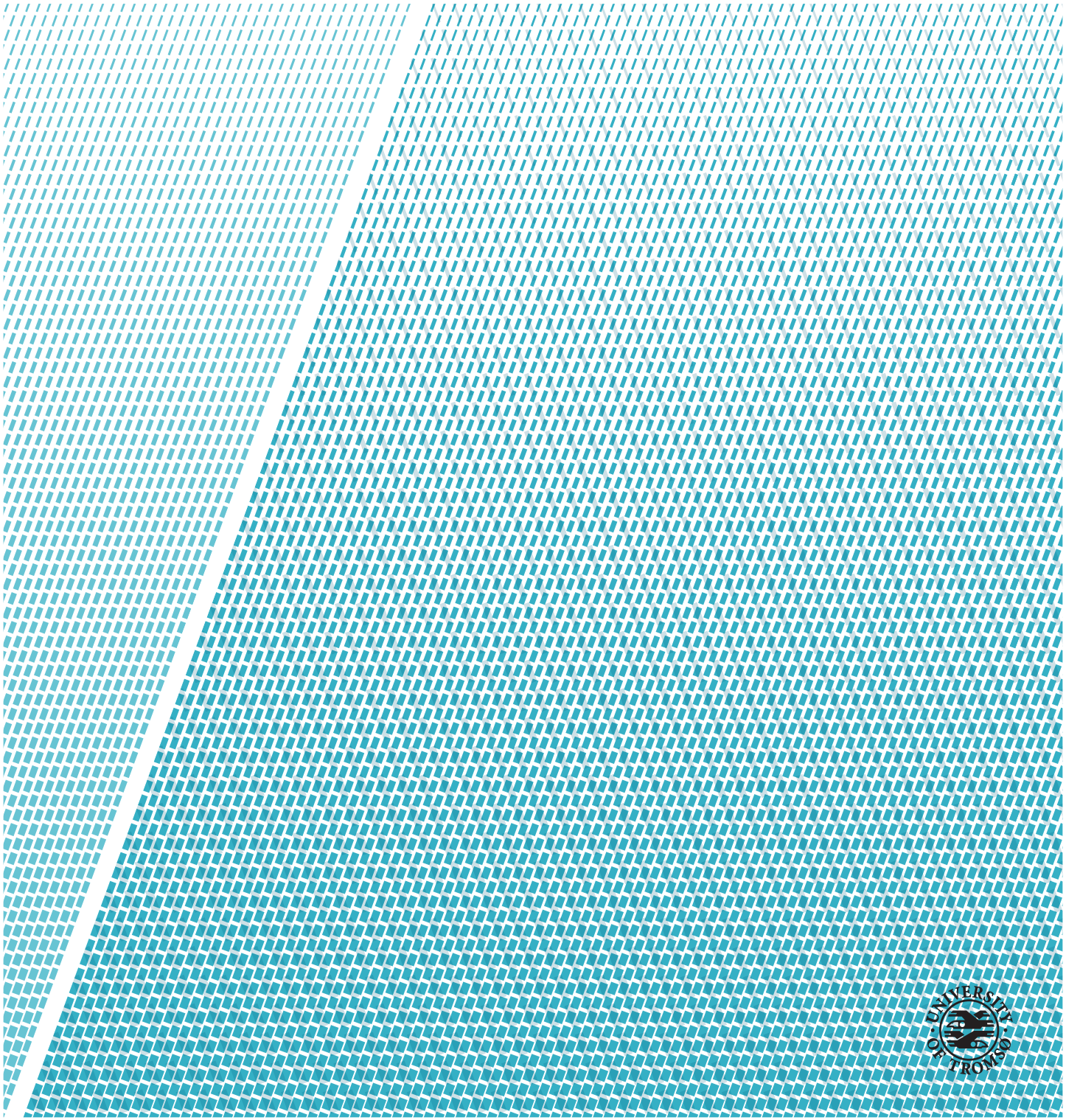

This thesis document was typeset using the *UiT Thesis LaTeX Template*.
© 2018 – http://github.com/egraff/uit-thesis

To my Mother and Father.

Thank you so much for everything.

Abstract

In this thesis, the reflectance was measured for angles from 10° to 80° for different n-type silicon based solar cells and for solar absorbers. The measurements were done with unpolarized, p polarized and s polarized light. The reflectance results show that both the solar cells and solar absorbers perform well under small variation from perpendicular angle well but as the angle of incidence increase substantially, the reflectance also increase significant. The Cary 5000 Spectrophotometer located at UiT the Arctic University of Norway was used to perform all reflectance measurements.

The thesis includes two comparison studies. The first compares how the solar position throughout the day during three different dates(15th of april, 15th og june and 15th of september) in Tromsø and Rome changes and affects the absorbance of a nickel aluminum solar absorber. The study shows that the solar absorber performs best in Rome in spring and autumn, while the solar absorber performs best in Tromsø in the summer. The second study uses angle dependent absorbance to see how much of the irradiance during the day that is lost. The day chosen was 17th of april, and the study shows a significant loss in irradiance as the day goes. The irradiance data used was retrieved from the Solar Edge monitoring system located at UiT.

Acknowledgements

The end of a five-year period in my life is nearly here. These five years have helped me grow as a person. It has been five years of hard work which I will never take for granted.

I would like to thank everyone that has helped me throughout the five tough years of studying. Whether it has been a study-related problem or a personal related problem, I have always had good friends around me for support. I am so grateful to you all.

I would like to thank my supervisor Prof. Tobias Boström for the help and guidance he has given me this year. It has been very important for me to have someone to lean on when problems have occurred. I would also like to thank Giuseppe Galbiati for providing me with solar cell samples.

Lastly, I would like to thank my family for their continual support for all these years. The support I have received from you have always been heartwarming.

Contents

List of Figures

List of Tables

Abbreviations

Abbreviation	Definition
TE	Transverse Electric
TM	Transverse Magnetic
AM	Air Mass
R & D	Research and Development
OPL	Optical Path Length
ARC	Anti Reflection Coating
STC	Standard Test Condition
EVA	Ethylene Vinyl Acetate
PDMS	Polydimethyl Siloxane
PVF	Polyvinyl Fluouride
PERC	Passivated Emitter and Rear Contact
PERL	Passivated Emitter and Rear Locally Diffused
PERT	Passivated Emitter and Totally Diffused
IBC	Interdigitated Back Contact
A-Si:H	Hydrogenated Amorphous Silicon
TCO	Transparent Conducting Oxide
CNT	Carbon Nanotube
UV	Ultra Violet
VIS	VISible
NIR	Near InfraRed
SiN_x	Silicon Nitrate
SiO_x	Silicon Oxide
TiO_x	Titanium Oxide
Ni_xAl_x	Nickel Aluminum

Nomenclature

Physical Constants

Symbol	**Description**	**Unit**
c	Speed of light in vaccum	$299,792,458 \mathrm{m/s}$
k_B	Boltzmann constant	$1\,38 \times 10^{-23} \mathrm{m^2 kg/s^2 K}$
h	Plancks constant	$6\,626 \times 10^{-34} \mathrm{m^2 kg/s}$

Other Symbols

Symbol	**Description**
λ	Wavelength
$R(\lambda)$	Reflectance
$A(\lambda)$	Absorbance
$T(\lambda)$	Transmittance
G(x)	Generation rate of electron
$\alpha(\lambda)$	Absorption coefficient
$\phi_p(\lambda)$	Photon flux per unit wavelength
I_{sol}	Solar Spectrum
I_p	Plancks black body radiation
α_{sol}	Normal solar absorption
σ_{therm}	Normal thermal emittance
E	Energy
E_G	Band gap energy
E_C	Conduction band energy
E_V	Valence band energy
n_x	Refractive index
n_{arc}	Refractive index of ARC
v_m	Speed of light in medium
Θ_i	Angle of incident
Θ_t	Angle of transmission
Θ_B	Polarization/Brewster's angle
δ	Declination Angle
β	Angle of inclination of the surface
ω	Hour angle
α	Elevation angle
ϕ	Latitudinal location on the earth from the horizontal
dy	Day of the year
R_s	Reflection coefficient of s polarized light
R_p	Reflection coefficient of p polarized light
d	Thickness of ARC
T	Temperature, in Kelvin

1 Introduction

As the world energy consumption continuously increase and the man-made climate changes has become a critical factor in the energy equation, renewable energy have become a major part in the modern development of energy in the recent decades. Solar energy has always been one of the biggest renewable energy sources because of the immense amount of energy that can be delivered from the sun, and the development does not seem to slow down.

As of today, the two most prolific ways of utilizing solar energy is photovoltaic cells and solar thermal collectors. Already being invented as a functioning photovoltaic(photocell) in 1954, photovoltaic has shown to be a crucial part towards a more sustainable future [Chapin et al., 1954]. From a conversion efficiency of approximately 6 percent through today where the conversion efficiency has increased to over 20 percent, photovoltaic has shown to be a reliable source of energy. Solar thermal technology is the second method of transforming solar energy to satisfy our needs and, as with photovoltaic, is already being used in households and in industrial complexes to provide energy. Unlike photovoltaic, which convert solar energy to electric energy, solar thermal collectors convert solar energy to heat and then warm up a medium that is transported through a heating system in a building.

The improvements of photovoltaic cells can be divided into two categories, electrical and optical. The electrical improvement, which we are not going to discuss in-depth in this thesis, focus on improvements with regards to series and shunt resistances, recombination and system problems. The optical focus

is the improvement of light absorption. One of the variables that is different world wide is the angle to which the sun light hit the surface of the earth. The sun light will hit the surface at a lower angle in Tromsø than in Barcelona, and investigating how both solar cells and solar thermal absorbers react when changing the angle of incidence of the sun light is important to understand and utilize them to their full potential.

1.1 Reflectance

The reflectance is one of the fundamental parameters to determine whether the solar cell or solar absorber is capable of displaying great efficiencies. For solar cells, the reflectance is for example one of the parameters in the generation rate equation,

$$G(x) = \int_0^{\lambda} [1 - R(\lambda)]\alpha(\lambda)\phi_p(\lambda)e^{-\alpha(\lambda)x}d\lambda \tag{1.1}$$

where R(λ) is the reflectance, $\alpha(\lambda)$ is the absorption coefficient and $\phi_{\mathrm{p}}(\lambda)$ is the photon flux, all as a function of wavelength. It is the cornerstone when it comes to determining the absorbance experimentally. For solar absorbers, the reflectance stand out in similar fashion like in the solar cell case but determining whether or not a solar absorber is efficient is a less complex affair. In solar cells and modules other factors come into play, such as electrical parts, before one can determine whether the solar cell is viable. For solar absorbers, the greatest importance is for the selective surfaces to generate heat with low radiative emission. This means that measuring the reflectance and quantifing the absorbance in solar absorbers will create a fuller picture of its potential than it will for solar cells. Providing the normal solar absorption equation(see section 2.1.1, equation 2.3) with the necessary parameters, reflectance and data of the solar spectrum, will then give a good pinpoint about the solar absorber.

1.2 Objective and Approach

The objective of this study is to investigate how the reflectance and ultimately the efficiency of solar cell samples and solar absorber samples is dependent on the incident angle of the incoming light. Usually when a new type of solar cell or solar absorber is optically tested it is only tested at perpendicular incident angle, and gives little data on how it performes when it is not perpendicular. Solar modules without 2-axes tracking system will rarely be exposed to a perpendicular incident angle of light so investigating the angle-dependency

will make up for a clearer view of how the solar cell or solar absorber perform in the real world.

The reflectance will be measured experimentally in renewable lab at UiT the Arctic University of Norway. All measurements are done by me and the Cary 5000 spectrophotometer was used for all measurements during this study.

2

Theory

2.1 Optics

Before the optical improvement methods are discussed, it is important to touch on some of the fundamental physical basics of the optics of solar cells and solar absorbers. The optical improvement methods are heavily depend on some of these fundamental building blocks and without them the efficiencies of solar cells and solar absorbers would not reach the height they are at. In order to not cause confusion they are presented in this section.

2.1.1 Optical Characteristics

The common quantities measured for both photovoltaic and solar absorbers are the absorbance, reflectance and transmittance. These quantities are all measured in percent. The absorbance is the quantity measuring how much of light is absorbed. Reflectance is the quantity measuring how much light is reflected off of the surface of the material. Lastly, the transmittance is the quantity measuring how much of the light is transmitted through the material. The relation between them is as follows,

$$A(\lambda) + R(\lambda) + T(\lambda) = 1 \tag{2.1}$$

Where A is the absorbance, R is the reflectance, T is the transmittance and λ is the wavelength(commonly given in nanometer when dealing with photovoltaic and solar absorbers). When creating a solar absorbers, the spectral selective film

is deposited on a $\sim$ 100% opaque substrate. This means that the transmittance throughout the material is approximately 0, and Eq. 2.1 can be reduced to

$$A(\lambda) = 1 - R(\lambda) \tag{2.2}$$

Normal solar absorption is defined as,

$$\alpha_{sol} = \frac{\int_{0.3}^{4.1} I_{sol}(\lambda)(1 - R(\lambda))d\lambda}{\int_{0.3}^{4.1} I_{sol}(\lambda)d\lambda} \tag{2.3}$$

where I_{sol} is the solar spectrum. The normal solar absorption is the ratio of the absorbed radiation and the incoming solar radiation. For solar thermal absorbers, there is a specific region where it is desirable to absorb photons and a specific region where it is desirable to repel them. The region of interest is the UV-VIS-NIR region, which in terms of wavelengths is 300-4100 nm. The integration boundaries of the normal solar absorption takes this into account(they are given in μm, which is easily changable). The normal thermal emittance is given by,

$$\epsilon_{therm} = \frac{\int_{2.5}^{20} I_p(\lambda)(1 - R(\lambda))d\lambda}{\int_{2.5}^{20} I_p(\lambda)d\lambda} \tag{2.4}$$

and is the ratio between the emitted radiation and Plancks black body radiation I_p. The normal thermal emittance describes the amount of heat generated by the absorber and is desirable to have as low as possible.

2.1.2 Photon, Phonon and Plasmon

As one of the essential building blocks in solar energy, and indeed a fundamental part in various fields of physics, are photons and photon absorption key elements of how solar cells and solar absorbers work. Phonons and plasmons are two other particles that have properties of interest for use in the photovoltaic and solar collectors. Whereas phonons are specific for indirect bandgap semiconductor, plasmons has important applications with regards to optical enhancement of solar cells and solar absorbers.

Photon

The photon is an elementary particle considered to have high energy and low momentum, and was most commonly found by Albert Einstein with his law of the photoelectric effect, being the essential discovery it was. The energy and

the wavelength of a photon is related as

$$E = \frac{hc}{\lambda} \tag{2.5}$$

where E is the energy of the photon, h is Plancks constant, c is the speed of light in vacuum and λ is the wavelength of the photon. The energy, most commonly expressed in joule, can also be expressed in electron-volt,

$$E = \frac{1.24}{\lambda}. \tag{2.6}$$

Electron-volt is the measure of the energy needed for an unbound electron to pass through a potential difference of 1 volt in vaccum, and is the common unit used for band energies. The electron-volt is merely a quantity created for convenience, rather than expressing the energy in joule where the numbers are cumbersome and small.

Phonon

In an indirect band gap semiconductors it is not only enough for the electrons to be hit by the photons of the desired energy to be excited to the conduction band, it also need the phonon to be excited. It is a two-particle dependent system. Phonon is a low energy and high momentum quasiparticle that "exist" in the material. Whereas the direct band gap semiconductors have the conduction band and the valence band aligned properly on top of each other with respect to a wave vector k(and only the photon is required in order to excite the electron), the conduction band and valence band of indirect band gap semiconductors are skewed and the high momentum phonon is required to excite the electron[Solanki, 2015a].

Another way of looking at phonons for a better understanding is to look at it from the perspective of waves. Sound waves are transported throughout a material, with low energy(long wavelengths). From the same perspective, heat is being transported through a material and this is what the phonon is. It is the motion/vibrations of the atoms, between themselves, in the crystal lattice. And so, with the energy from the photon and the heat motion within crystal lattice, the excitation of an electron occur. Silicon is an example of a semiconducting material that utilizes both photons and phonons to function as a solar cell.

Plasmon

Just like phonons, can plasmons be regarded as quasiparticles. It is the collective oscillations, or plasma oscillations, of the conducting electrons in a metal.

Plasmons occur in metal particles and have different properties depending on the size of the metal particles[Pillai et al., 2007]. Particles smaller than the wavelength of rays tend to absorb, enhancing the absorption properties of the material. Particles larger than the wavelength tend to scatter, contributing to the light trapping mechanism of the material. As discussed further in section 5.2, metal particles are undesirable in the layers above the absorbing surface because it may contribute to parasitic absorption. For solar cells, parasitic absorption refers to absorption that do not contribute to photo-generated current, but only result in thermal generation. This implicates that for plasmonic technology to be desirable in solar cells the size of the metal particles are crucial.

2.1.3 Refractive Index and Snell's Law

The refractive index of a material is the ratio between the speed of light in vacuum and the speed of light in a given medium, such as air. Mathematically, the refractive index is expressed as,

$$n = \frac{c}{v_m} \tag{2.7}$$

where n is the refractive index, c is the speed of light in vacuum and v_m is the speed of light in the medium. The refractive index determines the bending of light at the interface between two mediums. If the refractive index of the material is higher than that of air, the light refracted is going "downwards". If the refractive index of the material is lower than air the light is refracted towards the surface.

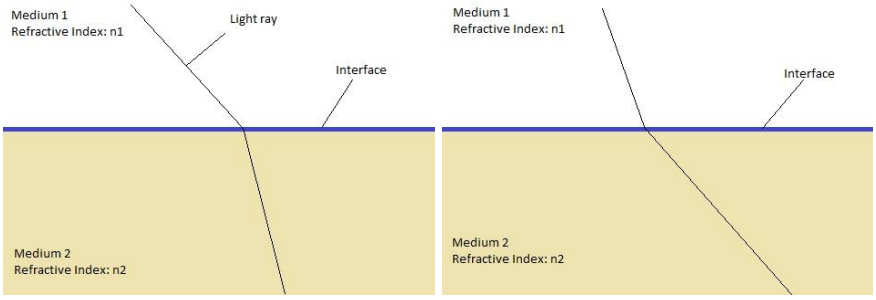

(a) Beam trajectory between two media where medium 2 has the largest refractive index

(b) Beam trajectory between two media where medium 1 has the largest refractive index

The refractive index is a useful tool when anti reflection coating is applied to a solar cell and is also the basis for Snell's law,

$$n_1 sin(\Theta_i) = n_2 sin(\Theta_t) \tag{2.8}$$

where n_1 and n_2 are the refractive indices, Θ_i is the angle of incidence of the light and Θ_t is the angle of the transmitted light.

2.1.4 Wave Theory - Fresnel Equations and Polarization

Sun light is considered to be electromagnetic waves and being an electromagnetic wave includes having an electric and a magnetic field and yields certain properties. One of which is polarization. In general, polarization is described to be the orientation of the electric and magnetic field of the wave. Light is considered to be unpolarized, which means that the angle to which the electric and magnetic field is oriented is random.

When the electric field vector is perpendicular to the incident, reflected and refracted plane, called s-polarization or transverse electric(TE) polarization, and when the electric field vector is in line with the plane, called p-polarization or transverse magnetic(TM) polarization. The reflection coefficient is a parameter dependent on whether it is transverse electric or transverse magnetic polarization and is given as,

$$R_S = \left(\frac{\sin(\Theta_t - \Theta_i)}{\sin(\Theta_t + \Theta_i}\right)^2 = \left(\frac{n_1\cos(\Theta_i) - n_2\cos(\Theta_t)}{n_1\cos(\Theta_i) - n_2\cos(\Theta_t)}\right)^2 = \left(\frac{n_1\cos(\Theta_i) - n_2\sqrt{1-(\frac{n_1}{n_2}\sin(\Theta_i))^2}}{n_1\cos(\Theta_i) + n_2\sqrt{1-(\frac{n_1}{n_2}\sin(\Theta_i))^2}}\right)^2 \tag{2.9}$$

$$R_P = \left(\frac{\tan(\Theta_t - \Theta_i)}{\tan(\Theta_t + \Theta_i)}\right)^2 = \left(\frac{n_1\cos(\Theta_t) - n_2\cos(\Theta_i)}{n_1\cos(\Theta_t) - n_2\cos(\Theta_i)}\right)^2 = \left(\frac{n_1\sqrt{1-(\frac{n_1}{n_2}\sin(\Theta_i))^2} - n_2\cos(\Theta_i)}{n_1\sqrt{1-(\frac{n_1}{n_2}\sin(\Theta_i))^2} + n_2\cos(\Theta_i)}\right)^2 \tag{2.10}$$

Where R_S and R_P are the reflection coefficients for s and p- polarization, respectively. Θ_i is the incident angle of the light, Θ_t is the angle of the transmitted light, and n_1 and n_2 are the refractive indices of the two mediums. These two equations are referred to as the Fresnel equations. The reflection coefficient describes the amplitude of the reflectance of an incident ray and the Fresnel equations describes the reflectance amplitude of a transverse polarization wave.

A consequence of the Fresnel equation is the phenomena called Brewster's angle, or polarization angle. The Fresnel equations are dependent on the refractive indices of the interfacing mediums and the incident angle of light. The polarization angle is the angle of incident where the polarized light is completely transmitted, hence no reflection occurs. The Brewster's angle can

be derived from Snell's equation and is given as,

$$\Theta_B = \arctan(\frac{n_2}{n_1}). \tag{2.11}$$

2.2 Solar Radiation

The sun is essentially a fusion reactor. As a fusion reactor it unleashes immense amounts of energy every second. A tiny amount of this energy radiates to earth. The radiation can be divided into different categories: i) extra-terrestrial radiation, ii) diffuse radiation and iii) direct/beam radiation. Extra-terrestrial radiation is the radiation that does not enter the atmosphere. The diffuse radiation is the radiation that is absorbed or scattered throughout the atmosphere. Direct or beam radiation is the light that hit the surface of the earth. Once the light comes through the atmosphere and hit the surface there is also a fourth factor called reflected radiation, or albedo.

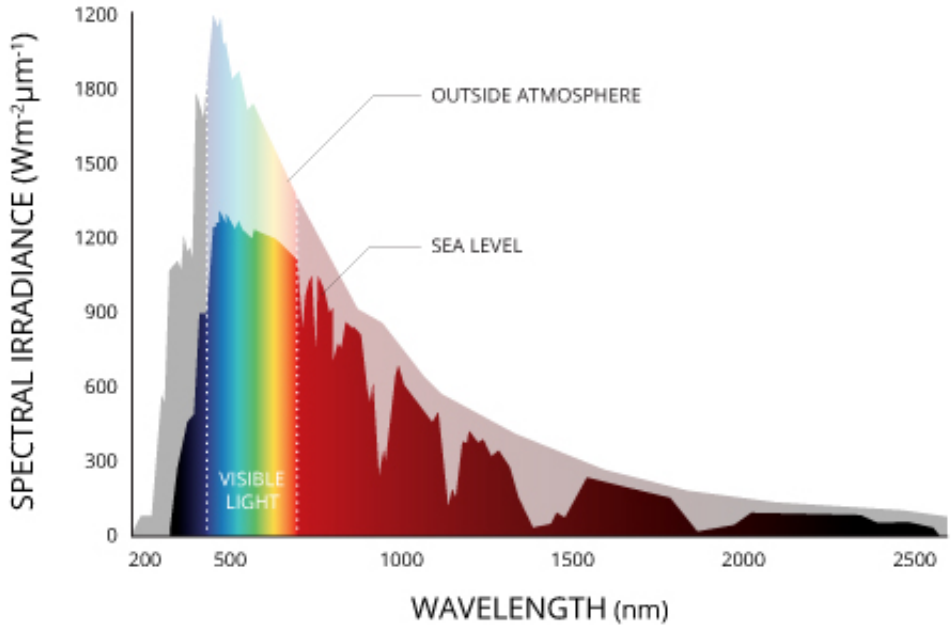

Figure 2.2: Irradiance of the solar spectrum with respect to wavelength[Fundamentals of Environmental Measurements, 2016].

Fig 2.2 show the difference of extra-terrestrial irradiance and direct/beam irradiance at the surface with AM1.5. As we see, there is a peek spectral irradiance in the visible spectrum, which indicates that most of the photons that hit the surface of the earth is in the visible spectrum.

2.2.1 Planck's Black Body Model

Planck's law was derived by Max Planck and shows how the spectral radiation, $B(\lambda, T)$, of a black body varies with the wavelength and temperature. Before

Planck derived the black body model, the current classical model at the time showed that the spectral radiance would go to infinity as the wavelength went to zero, which Planck proved wrong. Mathematically, the black body model is given as,

$$B(\lambda, T) = \frac{2hc^2\lambda^{-5}}{e^{\frac{hc}{\lambda k_B T}} - 1} \tag{2.12}$$

where λ is the wavelength, h is Planck's constant, c is the speed of light in a vacuum, k_B is the Boltzmann constant and T is the temperature in kelvin. Planck's black body model is used in emissivity studies(as touched upon in section 2.1.1) and is an important tool for understanding the radiation pattern of stars.

2.2.2 Air Mass

Air Mass is a ratio described by the incident angle of the light and the surface normal of the earth.

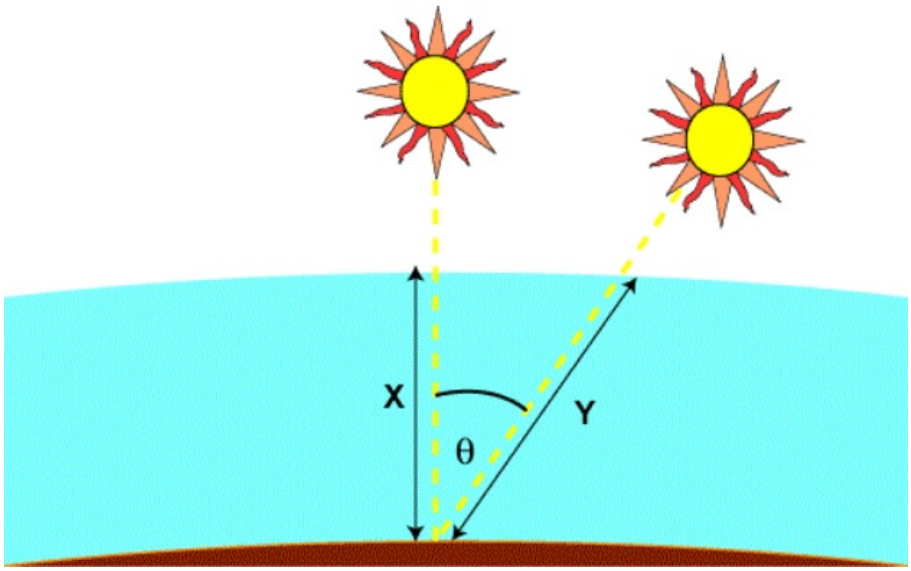

Figure 2.3: Depiction of how AM is defined [PVEducation, 2018].

Air mass is expressed mathematically as,

$$AM = \frac{1}{\cos \Theta} \tag{2.13}$$

where Θ is the angle between the light ray and the surface normal. Common air mass numbers are AMo which is extra-terrestrial and not inside the atmosphere,

AM1 is for light normal to the surface(0°), and AM1.5 is incident angle equal to 48 2°. The direct irradiance in fig 2.2 is given for AM1.5.

2.2.3 Angle of Incidence

When considering the angle dependency of a solar cell or solar absorber, several factors come into play(the tilt of the absorbing surface, the location on the earth, etc.). The angle of incidence is the main object to find when comparing the efficiency of the solar cells/absorber to data measured from the real world.

The declination angle is the angle bewteen the center of the sun and the center of the earth. Image an axis going through the center of the earth. The declination angle is the angle to which the center of the sun deviated from that axis.

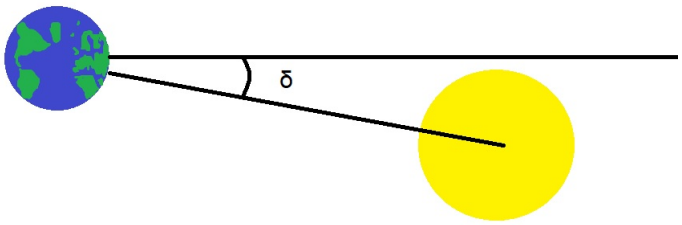

Figure 2.4: Illustration of the declination angle.

The declination angle is given in the equation below,

$$\delta = -23.45 \cdot \cos(\frac{360}{365} \cdot (10 + dy)) \tag{2.14}$$

where dy is the day of the year(1st of january is dy = 1). The hour angle is given in eq 2.15:

$$\omega = \sin^{-1}(\frac{\sin\alpha - \sin\delta \sin\phi}{\sin\phi}) \tag{2.15}$$

where δ is the declination angle, ϕ is the latitudinal location on the earth, β is the angle of inclinaton of the surface from the horizontal and α is the elevation angle(The angle between the horizontal surface of a given location on the earth and the sun).

For a tilted surface, facing directly south the following equation determines the angle of incidence,

$$\Theta_i = \cos^{-1}(\cos\delta\cos(\phi-\beta)\cos\omega + \sin\delta\sin(\phi-\beta)) \tag{2.16}$$

where δ is the declination angle, ϕ is the latitudinal location on the earth, β is the angle of inclinaton of the surface of from the horizontal and ω is the hour angle.

2.3 Optical Improvement Methods

The optical improvement methods for solar cells are mostly concerned with increasing the absorption of photons to produce electron-hole pairs, which in all reality is the main driving-force to make a good solar cell. For solar absorbers, where parasitic absorption is not an issue, the main target is to absorb photon in the most efficient way. With the technological improvement below is the reflection of the light almost zero, at least for normal incident. The following sections will present the most used optical improvement methods.

2.3.1 Surface Texturization

The concept of surface texturization is to manipulate the surface such that if the photon is reflected off the surface at the first encounter(or first bounce), the photon is reflected in such a way that it will be directed towards the surface once more - increasing the probability of the photon being refracted and absorbed by the material at a later stage. **The texturization causes the light to have multiple encounters with the surface**.

Surface texturization has been done in different shapes. The most common shapes for texturization, because of the organic bouncing mechanism and broad ways of manufacturing, is the pyramid and inverted pyramid formation. Simulation studies have been done to investigate the difference of the pyramidal bases(triangular, rectangular, pentagon) to investigate the optimal shapes[Hua et al., 2010]. The current shapes(triangular, square) can be produced with both dry and wet etching as well as microgrooving, making it easier to find an efficient way to incorporate it into the manufacturing process. Less common shapes are the honeycomb texturization, V-grooving and in the R & D stages are surface texturization in the shape from the nature, such as the moth eyes [Du et al., 2014; Willeke et al., 1992; Asadollahbaik et al., 2014].

The process of surface texturization is done mainly using etching techniques. These techniques are often divided into two categories, dry and wet etch-

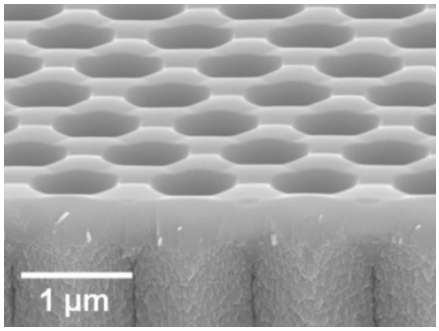

(a) Honeycomb structure[Du et al., 2014]

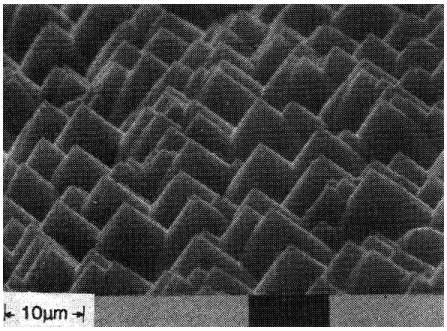

(b) Square pyramidal structure[Campbell et al.,1987]

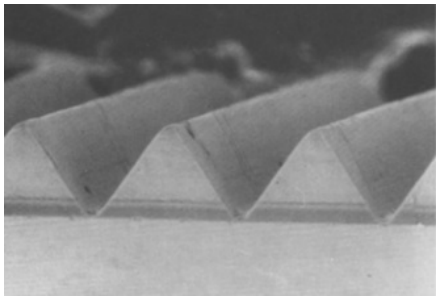

(c) V-grooving structure[Willeke et al.,1991]

ing[Moreno et al., 2014]. For wet etching, a hydroxide solution is used, typically KOH or NaOH[Singh et al., 2001], while for the dry etching techniques plasma or reactive ion etching method is used[Jansen et al., 2001; Moreno et al., 2010; Yoo, 2010]. The main object of the etching methods is the same. It is to create an uneven surface that has the ability to redirect photons towards the surface if it is not refracted at first impact, thus increasing the probability of being absorbed.

2.3.2 Anti Reflection Coating

Anti reflection coating(ARC) is a dielectric layer deposited on the surface of the solar cell. It has the properties of not absorbing light, which potentially could contributing to parasitic losses, for solar cells, on the surface and reducing the reflected light. A reduction in reflection is caused by creating a destructive interference between the incident and reflected light. This is done by choosing the correct thickness d and refractive index n_{arc} of the ARC. The thickness of the ARC is given as,

$$d = \frac{\lambda_0/n_{arc}}{4} = \frac{\lambda_0}{4n_{arc}} \tag{2.17}$$

The thickness from Eq. 2.17 is wavelength dependent and governs only one single wavelength. The ARC thickness should then be chosen in the interval where the the solar intensity is highest, which is between 500nm and 600nm.

Because of the glass substrate that is placed on top of the solar cell, the reflection in the ARC and semiconductor is slightly affected. The refractive index of the ARC when has to be changed for minimum reflection which is given by,

$$R_{min} = \left(\frac{n_1^2 - n_0 n_2}{n_1^2 + n_0 n_2} \right)^2 \tag{2.18}$$

The minimum reflection will evidently be zero if the following condition is met,

$$n_1 = \sqrt{n_0 n_2} \tag{2.19}$$

where n_0 and n_2 is the refractive indices of the semiconductor and glass, respectively[Solanki, 2015b].

The main optical difference between surface texturization and anti-reflection coating is that the surface reflection is directly reduced with ARC using the destructive interference, while for surface texturization the surface reflection is not reduced directly. The probability of the light being refracted is increased because of the bounces.

2.3.3 Surface Plasmonics

Surface plasmons has, in some form, been known for over a century and in recent development of optical improvement methods it has started to show result in terms of efficiency[Wood, 1902].

As mentioned earlier, surface plasmons are used to scatter the incident light and enhance the light trapping(in the solar cell device). Surface plasmonics is a cross-over between passivation and light trapping in a sense that the metal particles used, mostly commonly silver and more rarely gold, are embedded in a passivation layer and its overall mechanism is to scatter light for light trapping. The delicate matter of using these metal particles is to not have them too small, ending up absorbing the light and creating a radiation process which is undesirable, and not have the particles too big and cause scattering effects in the device.

For solar absorber, which do not have the cumbersome problem of parasitic absorption, uses the surface plasmons to absorb the incident light rather than using them to scatter. Because of the less restricted use of surface plasmons, almost any particular metal can be used.

The main mechanism for surface plasmonics lays in the resonance effect that occurs once the light has hit the surface of the module. As the light hit the metal particles in the dielectric passivated layer, the movement of the conduction electrons, in the metal particles, upon excitation with the incident light leads to a build up of the separation of positive and negative charges induced per unit volume of the passivation layer. This acts as a restoring force, allowing a resonance to occur at a particular wavelength. This wavelength is called the **dipole surface plasmon resonance frequency**. The incident light that is in the vicinity of this resonance frequency is strongly scattered throughout the material.

The last two optical improvement methods does not apply to solar cells.

2.3.4 Passivation

Because of the cut done to the wafers in the manufacturing, a critical interruption in the crystal structure occurs. This interruption produces a destructively high defect density in the material, which influences the efficiency. Once the cut is done, the high defect density creates a high parasitic absorption and high recombination rate at the surface.

The most widely used application for this problem is to passivate the surface of the material. The basic principle of passivation is to introduce atoms, such as oxygen and nitrogen, to the surface where the cut has happened. These atoms bind themselves to the surface atoms and the defect density decrease. Passivation of the surface becomes a film that coates the surface and binds the atoms at the surface of the material which are cut off the crystal lattice, and are not inter-connected with atoms in all directions. Popular passivation films are SiN_x, SiO_x and TiO_x.

2.3.5 Light Trapping

In recent year, investigation of reducing production cost have been one of the important topics of solar cell manufacturing. One of the ways of reducing the production cost is to produce thinner wafers, which subsequently requires less material. A consequence of this material reduction is that light has a smaller amount of material to travel through to be absorbed. Optical path length(OPL) is the term used to describe the length the rays travel within the material. For a straight clean wafer with no surface texturization and a perpendicular beam the OPL is the thickness of the material. The OPL can be increased, and this is called light trapping.

As was hinted in the previous paragraph, surface texturization is paramount for light trapping, or for the OPL to increase. Both front and back surface can be texturized for the light to bounce off the front surface, and also if the beam is transmitted through the material has the opportunity to bounce at the back surface. The OPL is increased at first encounter to the front surface by angling the light from the front surface, and further increased by letting it bounce back from the back surface.

2.4 Solar Cells

As one of the most developed technologies within the renewable energy branch, photovoltaic has played a major role in fight for a more sustainable future for decades already. The photovoltaic and solar cell technology is continuously improved and we see commercial interest worldwide, especially in Asia [Jäger-Waldau, 2016]. As of late, thin-film technologies such as the Perovskite and hydrogenated amorphous silicon solar cells have started to challenge the ordinary silicon wafer solar cells with their advantages in material reduction and increased conversion efficiencies of over 20 percent.

The section will give a superficial overview of how photovoltaic work and the module structure of the solar cells, as well as introducing come well-established technologies and some new concepts in photovoltaic.

2.4.1 Photovoltaic

The fundamental part of the solar cell is carrier(hole and electron) and voltage/current generation. It is a process that start already at the selection of semiconductor and continues all the way through to the delicate optical technicalities. Below is a brief description and explanation of photo-generation.

Properties of Semiconductors

An important characteristic of materials is how the energy band lay in relation to each other. There are three types of material: insulator, conductor and semiconductor. An insulator has a very large gap between the conduction band and the valence band, so electrons very rarely are in the conduction band. In a conductor, the conduction and valence band often overlap or the are sufficiently close so very little energy is required to excite electrons. It was discovered that some types of materials, called semiconductors, have a gap between the two energy band that is not too big nor too small. This implies that a certain

amount of energy can be applied to excite the electron from the valence band to the conduction band. So to be specific, in order for electrons to occur in the conduction band, they have to be excited by some form of energy. At 0 K(absolute zero temperature), all electrons are in the valence band. To fit the application of a solar cell, the gap of the semiconductor needs the size that when the material is exposed to natural energy(i.e. sun light), the electrons can be excited.

Energy Band and Band Gap

The essential property of semiconducting materials is that the gap between the energy bands is neither too big(like an insulator) nor too small(like a conductor). In order for an electron to be excited from the valence band to the conduction band a certain amount of energy is needed. Energy in form of photons from sun has shown to have energies sufficient enough to excite electrons, and thus creating electron-hole pairs in the material. For semiconducting materials used for solar cells the energy needed to excite an electron is given as,

$$E_G = E_C - E_V \tag{2.20}$$

where E_C is the the energy of the conduction band, E_V is the energy of the valence band and E_G is the energy of the band gap between them and subsequently the energy needed to excite an electron. For an electron to be excited E_G is the minimum energy needed. If an electron encounters a higher energy photon it gets excited but the excess energy is radiated from the material in the form of thermal energy.

PN-Junction, Doping and the Depletion Region

To enhance the semiconductors in terms of being used for solar cells they are being ”doped”. Doping is a process that introduce other atoms with fewer and/or more electrons in the outer shell to the semiconducting material. For example, silicon has traditionally been doped with boron and phosphorous to create an area with more holes the, called the p-type side, and an area with more electrons, called the n-type side, respectively.

When the p-doped material and the n-doped material are merged together the excess holes in the p-doped material will be attracted to the n-doped material and visa versa. The holes will then start stacking on the n-side, while the electrons start stacking on the p-side. The holes and electrons will leave behind uncompensated donors(acceptor donors from holes, and ionized donors from electrons), which will induce an electric field over a region. This region

is called the **depletion region** or **space charge region**. The regions outside of the depletion region is called the quasi-neutral region.

Photo-Generation

When the solar cell is exposed to illumination from the sun, generation of charge carriers begins, in what now is called a non-equilibrium condition/state for the solar cell. Photons hit the solar cell, are absorbed by the material and electron hole pairs are created. Two characteristics determine whether the generated electron hole pairs contribute: i) The diffusion length and ii) the recombination. The recombination rate is the materials natural way of restoring equilibrium and work for the electron to go back into the valence band after being excited. The diffusion length is also a material property and is the length of which the electron can go before it recombines. When diffusion length is large and the recombination rate is low, the probability of the carriers to contribute to generation is high. It implies that if recombination rate is high and diffusion length is low, the probability for generation is low.

There are two different generation processes in the P-N junction and the solar cell, i) photovoltage and ii) photocurrent. The photovoltage is generated as carriers are produced from illumination and electrons start stacking on the N-side, and holes start stacking on the P-side. The overall potential difference between N-side and P-side is the photovoltage. As carriers wander through the depletion region after begin generated contribute to the photocurrent.

Appropriately, materials with band gaps in the vicinity of the majority of photons radiating from the sun are used as the bulk material for solar cells. Once it is properly doped and contacts are incorporated into the material, a functioning solar cell is in place.

2.4.2 Standard Module Structure

In the development of solar cells they have to be able, among other things, to withstand a standard test conditions(STC) in order to be viable for commercial use. A solar cell alone, or a solar module for that matter, does not handle the natural conditions by themselves so protective layers are added to the module to secure that the solar cells are not damaged or destroyed in a matter of days or months. The module structure is shown in fig 2.6 and has commonly the following layer structure: i) rear cover, ii) encapsulant, iii) solar cells, iv) encapsulant and v) glass cover.

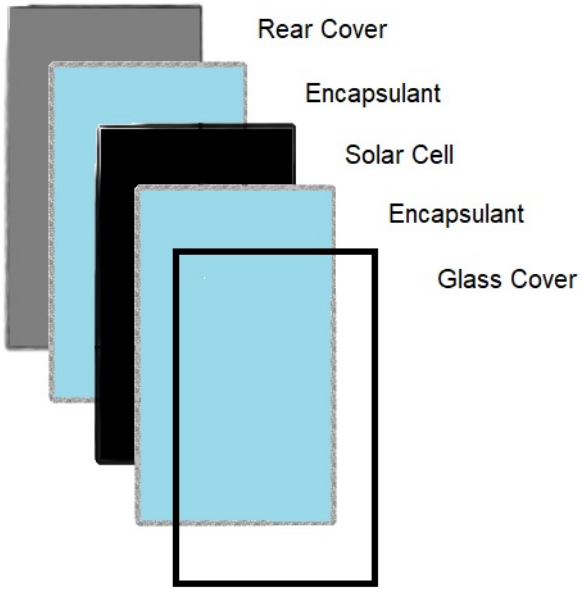

Figure 2.6: Typical layering in a standard solar cell module

A rising problem of adding layers in front of the solar cell is that these new layers can enhance reflection of sun light or contribute to parasitic absorption. This is undesirable and a narrow selection of materials is at disposal to evade this.

Glass Cover

The "top" layer in the module structure is a glass cover. Even though the glass covers main function is to stabilize and protect the rest of the module

from weather, it should also to have some optical specifications. The glass should be textured and it should also have a low iron content. The low iron content because of the possibility of having the iron molecules absorbing the incoming light, which is undesirable. High transmittance is desirable for the glass cover.

Encapsulant

The encapsulant is the next layer in the structure, as well as the second to last. The desired properties of the encapsulant are i) high electrical resistivity, ii) low water absorption ratio, iii) high transmission and lastly iv) low melting temperature. The high electrical resistivity is present to have low electric losses from the solar cell. The low water absorption ratio is an extension of the function of the glass cover and helps to repel water which can damage the solar cell. High transmission is to keep the parasitic losses low, and lastly the low melting temperature is for the manufacturing process.

Whereas the glass- and rear cover are distinct layers in the structure, the solar cell layer is incorporated into the encapsulants, which surrounds the solar cells. Enclosing the solar cells further protects it and also takes care of other molecules or atoms to get to the solar cells, which in turn can damage it. Polydimethyl siloxane(PDMS) was predominantly used in the early days of solar cell technology, but as of late the typical encapsulant used is ethylene vinyl acetate(EVA). Studies have shown that EVA has some problems with regards to acidic production as well as having chemical stabilizers, and also that silicon-based encapsulant can enhance short-circuit current of the module[Kempe et al., 2007; McIntosh et al., 2009]. [Kempe, 2010] shows that PDMS has a lower absorptivity and a higher transmittance than the EVA, favouring the PDMS, but because of production and material cost is the EVA more commonly used in the later years.

Rear Cover

With similarities to the front glass cover, the rear cover has main function of repelling external factors. The rear cover should not be not inflammable, so high temperatures can occur without burning off the components or layers, which is a logical property when dealing with equipment which is staying in the sun for a long period of time. The rear cover should also vapour resistive. Polyvinyl Fluouride(PVF) has been the dominant rear cover material, which is a polymer material.

2.4.3 Bifacial Module Structure

An alternative to the standard solar cell structure is the bifacial solar cell structure. The main difference between the standard module structure and the

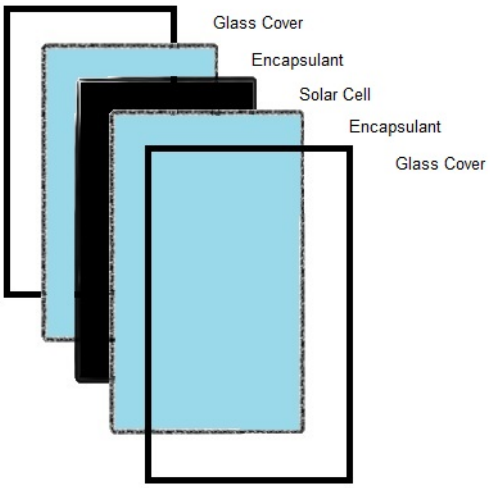

Figure 2.7: Layering of a bifacial solar cell module.

bifacial is the rear cover, which for bifacial is a glass cover. The bifacial structure can be utilized from both sides without changing the efficiency of the module. In the higher latitudes, the temperatures are generally lower for most of the year compared to the lower latitudes. Because of this, there is generally more snow in the higher latitudes. The bifacial modules utilizes the snow the way that if some of the irradiance does not hit the module, the reflection from the ground works as a reflection plate for the solar module and the light has another chance of absorbing the photons. In the summer, especially in the very high latitudes where there is midnight sun, the azimuthal angle of the sun on the sky is very varying. So, if the solar module is stationary mounted(no tracking system) at an angle(this means not flat on a wall or a roof) the solar module can utilize the sun over the course of the whole day from both sides.

2.4.4 Silicon Solar Cells

Silicon was in the beginning primarily used in the development of micro-electronics and circuitry surrounding this. One of the most noticeable negative sides of the use of silicon in micro-electronics was the waste. The silicon waste from the micro-electronics industry was found to be re-used as material for solar cells. Silicon is an indirect band gap semiconduction with a band gap of 1.14 eV. As discussed in 2.3.2, indirect band gap means that the electron not only need a photon to be excited. It also needs phonons in order to contribute to the generation of photo-current.

Silicon solar cells in their simplest configuration is called the n-type or p-type silicon solar cell. N-type or p-type because it describes the base type in the cell. In terms of amount in the solar cell, the base is the bulk of the semiconductor in the solar cell. These kinds of solar cells can be looked at as the blueprint of silicon solar cells and are often used as reference for testing new concepts.

PERC and PERL Solar Cells

Passivated Emitter and Rear Contact(PERC) solar cells is traditionally a silicon solar cell. As the name suggests, the main different from PERC to normal c-Si solar cells is that the emitter layer and the rear contact is passivated. A dielectric layer is deposited between the back/rear contact and the silicon layer and over the emitter layer in front. The Emitter layer is also heavily doped in the circumference of the front contacts.

Passivated Emitter and Rear Locally Diffused(PERL) solar cells is very similar to the PERC structure. Whereas PERC ”only” have heavy doped areas in the emitter, PERL solar cells also has heavy doped regions in the wafer near the rear contacts. PERL solar cells also have both passivated layer in the front and the back

IBC Solar Cells

Interdigitated Back Contact(IBC) solar cells have been the answer to a the question, "How do we come about removing the optical losses caused by contact shading?". It incorporates a texturized surface with passivation and ARC layers and has solely contacts on the back side of the solar cell, getting rid of any shading losses caused by the front contacts. Zero shading losses gives an increased photo generated current, which again increases the overall efficiency of the solar cell. The rear side contacts have interdigitated polarity, and the

emitter layer of the solar cell is now placed on the rear side as well, between the contacts and the base.

IBC solar cells give multiple advantages compared to the regular p-type or n-type solar cell. As mentioned before, there is zero shading losses from front contacts. Because of the new placement of the front contacts to the back there is no longer any need to be careful about the opticals regarding the grid, so the quality of the grid system can be enhanced. Studies have been done investigating the spectral response of IBC solar cells and found that they exhibit the highest spectral response over the full wavelength range among all c-Si solar cells[Ingenito et al., 2015]. Even though IBC solar cells are an aspiring silicon technology, there are some drawbacks that need to be taken care of. The IBC solar cell require multiple high temperature steps, which in turn cause an increased processing time, higher cost, increased chance of contaminations in the material. Laser doping has been proposed as an method of simplifying the processing sequence[Chan et al., 2012].

A-Si:H solar cell

Hydrogenated amorphous silicon(a-Si:H) solar cells is the last silicon based solar cell that is discussed.

The crystal structure of silicon is categorized in three different types, i) Mono crystalline, ii) Poly/Multi crystalline and iii) Amorphous. Mono crystalline silicon is a single lattice, while multi crystalline silicon are multiple lattice together. Amorphous silicon is a structure where the atoms have no particular order. Because of this, amorphous silicon was rarely used in the early develop-

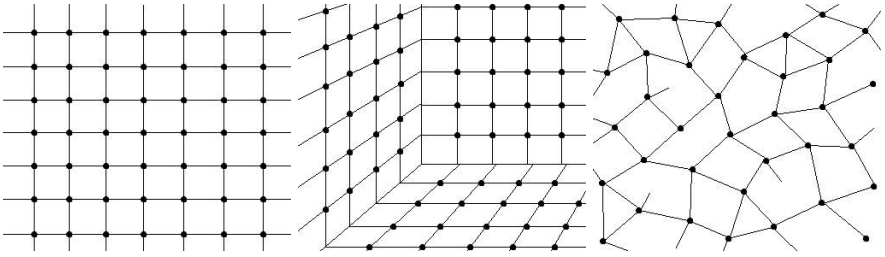

Figure 2.8: Illustations of the three different lattice structure of silicon mono crystalline, poly/multi crystalline and amorphous silicon respectively.

ment of silicon solar cell. The non-lattice structure showed to contain a lot of dangling bonds, causing undesired parasitic absorption. It was later discovered that passivating the dangling bonds, enhanced the amorphous silicon greatly and was then viable to use as a solar cell material. The passivation was done using hydrogen, and showed to have a better absorption than regular silicon

wafers. The enhancement of the amorphous silicon has given especially one significant contribution to the silicon solar cell technology. It has opened to make thinner silicon solar cells. Thinner silicon solar cells have the large benefit of having reduced material cost. The thinner solar cells are often categorized to be thin-film technologies, or 2nd generation solar cells. As one might resonate, the importance of light trapping and ARC is crucial for thin-film technologies to work.

2.4.5 Chalcogenide Solar Cells

As part of the second generation solar cells, chalcogenide solar cells have been part of the development of modern solar cell. The basic construction of the chalcogenide solar cell is the following: One layer of substrate/superstrate, an absorber layer, a window layer. The window layer is built up by two components, a buffer layer and a transparent conducting oxide(TCO) layer. Whereas the absorber layer is a p-type, the window layer is n-type. One of the things that separates the different chalcogenide solar cells in the deposition method. Some cells, like the $Cu(InGa)Se_2$ and $Cu_2ZnSn(S, Sn)_2$ based solar cells, are grown the same way the as regular silicon solar cells, with a substrate and back contact, with the absorber and window layer following, and some cells(CdTe are grown the other way around starting with the window layer and finishing with the base, called the superstrate-configuration. As part of the second generation solar cells, are the chalcogenide solar cells thin film, giving the advantage of lowering material consumption and cost. Since the material used also is abundant, it has a large potential of commercial use. An incredible opportunity for chalcogenide solar cells to conquer new ground in terms of application is that it has bring forth to use polymer as substrate producing flexible solar cells, which is far superior to the silicon solar cells when it comes to flexibility.

2.5 Solar Thermal Collectors

The second most prominent way of utilizing solar energy is by solar thermal collectors and one of the most important and essential part of the solar thermal collectors is the solar thermal absorbers. Unlike photovoltaic, which utilize energy from the sun to excite electrons to create electrical energy, solar thermal absorbers utilize the energy from the sun to heat water or a medium which in turn is used to heat the water in the water tank or heating system of a household or industrial complex.

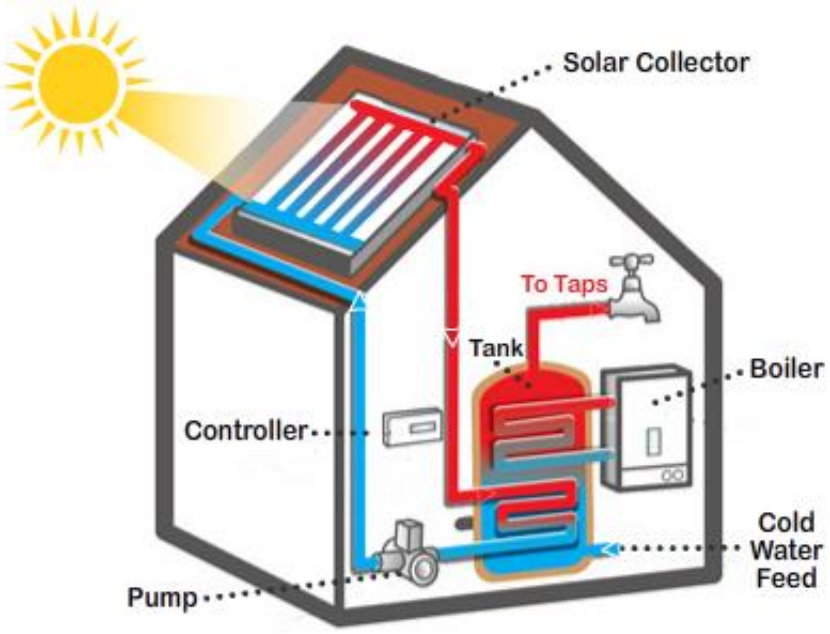

Figure 2.9: Solar collector system [EFCsolar, 2016].

There are different kinds of solar collectors systems, such as flat plate collectors, evacuated tube collectors and reflector systems. Even though the end product of these systems are the same, to heat the water supply of the system, they operate on different conditions. The flate plate and evacuated tube collector system are often the "go to" when a solar thermal collector is used in households. They operate as closed systems that use solar absorbers to heat a liquid which is when again used for heating the water tanks. The reflector system use reflective surfaces, often in parabola shape for increased efficiency, to concentrate the incoming sunlight and heat water. As this thesis governs solar cells and solar absorbers, the reflector system is not further discussed.

2.5.1 Flate Plate Collector

The flate plate collector is the solar collector that most people associate with. Its construction is based on the following five components: i) glass sheet, ii) flow tubes, iii) absorbers, iv) header and v) insulator. The glass sheet is the protective surface for the solar collector. The flow tubes contains the medium that is heated by the absorbers, which all collectively goes to a header and is then later pumped to a watertank or heating system. The function of the insulator is to retain the heat produced by the absorbers within the system so it is not wasted to the surroundings.

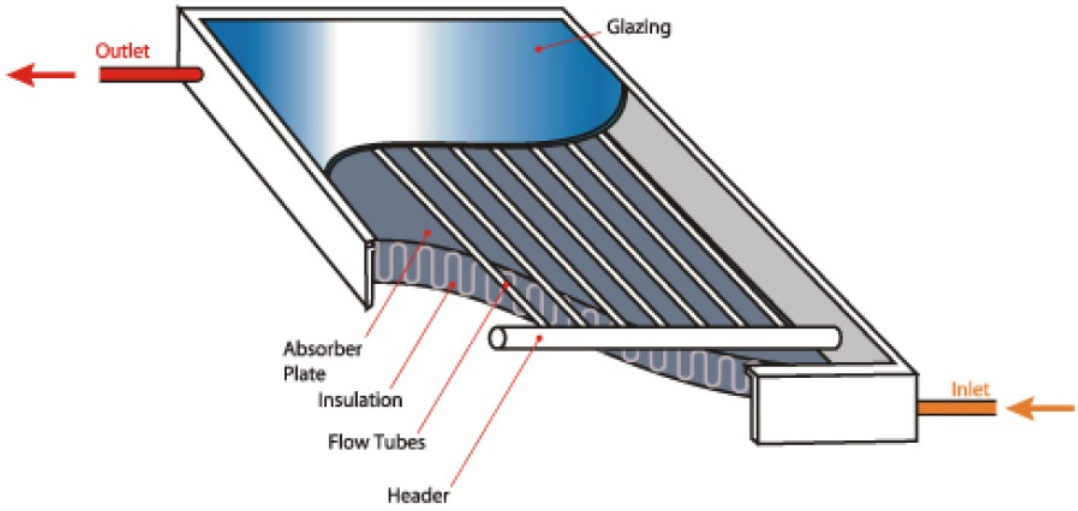

Figure 2.10: Flate plate collector [Steam of Boiler, 2018].

2.5.2 Evacuated Tube

The evacuated tube collector has similar characteristics to the flate plate collector, but some differences are evident. The heat pipes and absorber are separated into single tubes. The evacuated tube is a transparent tube that, with the absorber plate, heat the medium in the heat pipes. When the liquid inside is heated it will rise. The risen, boiling liquid is then placed inside the manifold where the liquid to the water tank or heating system is. Because of the separated circular tubes, the sunlight will always hit the surface of the evacuated tube perpendicular.

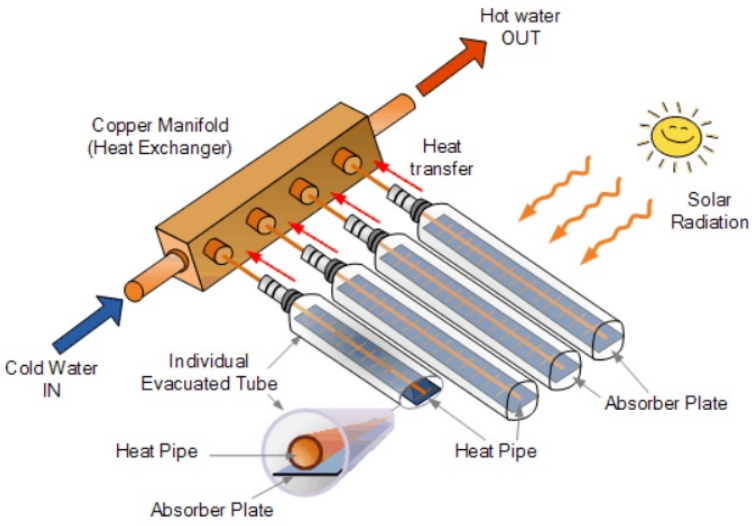

Figure 2.11: Evacuated tube collector [Alternative Energy Tutorials, 2018].

So the main difference between flate plate and evacuated tube collector is the following. The flate plate collector is a single-closed system and the evacuated tube collector is a double-closed system. Single-closed because the flow tubes are heated by the absorber plate, then transferred to the mechanical system. Double-closed because the heat pipes are first heated, which in turn heat the liquid that goes to the watertank.

2.5.3 Solar Thermal Absorbers

The solar thermal absorber is the main tool in a solar thermal collector system. The absorber is the part of the collector where solar radiation is absorbed and transformed into heat which is heating up the liquid in the pipes connected to the system.

The basic construction of an absorber is a base which is a high heat conducting metal, such as aluminium, and a layer of spectral selective material that has a high absorption coefficient in the visible spectrum and high reflectance in the infrared spectrum. When radiation from the sun hits the solar collector, it is absorbed by the spectral selective material. The heat generated is transported to the pipes using the highly heat conducting metal. The pipes are connected to the heat tank of a household or connected to some other heating system.

It may seem counter-intuitive to have a high reflectance in the infrared spectrum because you would like to use as much energy from the sun as possible, but the infrared spectrum mainly contribute to thermalization losses in the device and is not desirable in the development of good and commercial-competitive

absorbers. The heat-conducting metal is then connected to a set of pipes that are filled with liquid.

The following sections cover some of the common solar absorbers[Bermel et al., 2012].

Intrinsic Absorber

The intrinsic absorbers consist of some naturally spectrally selective material, deposited on a substrate. In order to have an ideal absorber it is preferable to have high absorptivity in the visible range, and high reflectivity in the infrared range of the solar spectrum. Intrinsic absorbers have shown to produce non-optimal because of the restrictions from the fact that one material is deposited on top of the substrate.

Textured Surface

With great similarities from the texturization of solar cells, the textured surfaces for solar absorbers act in the same way and "lean" on the light trapping mechanism that occurs once the light hit the surface of the absorber. If the initial hit is not absorbed the light bounces, is re-directed towards the surface and gets another chance of being absorbed. Unlike the other absorber structures, the textured surface is not deposited on top of a substrate. The structure is purely metal.

Semiconductor-Metal Absorber

Like the textured surface, semiconduction-metal absorbers have similar characteristics to solar cells, and can be considered to be the "solar absorber counterpart". Here, a semiconductor is deposited on top of a reflective surface and is coating by an anti reflection coating. This structure opens up for high absorptance in the UV and visible range because of the semiconductor, and high reflectivity of the longer wavelengths(infrared) because of the reflective surface, which usually is a metal. Because of the high reflection caused by the semiconductor, an anti reflection coating is layered on top.

Metal-Dielectric Composites

Metal-dielectric composites, also known as cermets, are metal nano particles embedded in a dielectric deposited on a substrate. The construct is much like

the semiconductor-metal absorber where the base functions as a reflector for the IR-wavelengths, the metal-dielectric absorbs UV-vis wavelength light. It is also common to have an anti reflection coating to lower the reflection. The metal-dielectric layer can be arranged in mainly two different ways, i) grading the nano-particle concentration with height in one layer, or ii) having to distinct layers in which the nano-particles are uniformly distributed within the layer, but the particle concentration is different. This implies having a structure with where the layer with highest concentration of particles is between the reflector and the lower concentration layer.

3 Method

During this study, the Cary 5000 spectrophotometer was used. With the Cary 5000, the Universal Measurement Accessory(UMA) was used. The Cary uses the software “Cary WinUV” which provides all the necessary programming options for the measurements. It gives the flexibility to change all parameters with a computer(except changing sample), rather than having the problem of changing parameters and positions as a sample is measured. This gives stability to the results obtained by the detectors in the spectrophotometer.

The UMA is a measurement accessory of the Cary. In order to investigate the angle dependency of incident light thoroughly, the equipment needs to have angle-flexibility. The UMA satisfies the needs of this study with the option of measuring the specular reflectance from the wide range of $5 - 85°$. The Cary is programmable to measure the reflectance from a desirable wavelength interval, at wavelengths varying from $190 - 2800$nm and gives the option of choosing between unpolarized light, p polarized or s polarized.

3.1 Samples

This study incorporates reflectance measurments of both solar cells and solar absorbers. The solar cells used were mainly based on silicon with different cell types, while the solar absorbers are mainly selective surface based on nano structures with aluminum back plate. In order to fit inside the UMA, the

samples were restricted in size and vary from 3x3cm^2 to 9x5cm^2.

3.1.1 Solar Cells

Two different types of silicon solar cells were used in this study, n-IBC and n-PERT solar cell. They are n-type based silicon solar cell.

The study includes two different n-IBC solar cell samples. The n-IBC1 is a solar cell with standard EVA as encapsulant and a standard glass as glass cover. n-IBC2 is a solar cell with standard EVA as encapsulant and has ARC -glass. The thickness of the glass was 3.2 mm for both n-IBC samples. PERT(219) has standard EVA and standard glass(3.2 mm).

All solar cell samples was provided by International Solar Energy Research Center Konstanz [ISC Konstanz, 2018].

3.1.2 Solar Absorbers

Five different solar absorbers were used in this study, and are mostly based on nano structures.

The CNT sample is a selective surface with carbon nanotubes(CNT) based surface and an aluminum backplate [Chen, 2016]. The Ni_xAl_x and the Sun-Strip(1 and 2) samples are solution-chemically spectral selective surfaces with nickel-aluminum nanostructures with an SiO_x ARC on a aluminum back plate [Boström, 2006]. The layering structure and the concentration of nickel nanoparticles differ in the samples, producing unique measurement results. The Alanod sample is a cromium oxide and cromium nitrate($Cr_2O_3/Cr(NO_3)_3$) layered surface with a aluminum back plate.

3.2 Measurement Approach

In this section the measurement method is explained and problems encountered with the measurements are discussed. Lastly, the use of the reflectance measurements are explained.

3.2.1 Step-by-Step

The initial stage of the measurements was to set up the Cary. The machine was turned on and the “Align” application in the "Cary WinUV" folder was started. In “Align” the lamps are set up and the UMA is connected to the Cary. The “Scan” application was then opened. This application is where all parameters are set, adjustments are performed and where the measurements are done. After “Scan” was opened the parameters are determined in “setup”. Altering from the default setting of the Cary, most of the setups were done in "Cary Options", "Baseline" in the instrument settings folder and "UMA" in the accessories folder. In "Cary Options" the default setup was 300-800 nm in the "X mode" and "Abs" in the "Y-mode". The wavelength was set depending on whether the measurements were done for solar cells or solar absorbers. Whereas the photon absorption in solar cells occurs from the size of the band gap level and above(in terms of energy), the photon absorption in solar absorbers occur at all wavelengths and importantly, all energy per photon is utilized. This set a certain boundary to the measurements of the solar cells. The measurements of the solar cells were done on the wavelength interval 300 – 1300nm. Both solar cell types used, n-IBC and n-PERT, are based off of silicon. Silicon has a band gap of 1.14 eV or just under 1100nm, so measurements of longer wavelengths is unnecessary as they will not contribute to the photovoltaic effect. Solar absorber samples were measured on the wavelength interval 300-2500 nm. The solar spectrum extends further than 2500 nm and the Cary has a photometric performance higher than 2500 nm, but the UMA showed poor measurement results with unreasonable reflectance values for the longest wavelengths, so the interval was narrowed down. The "Y-mode" was set to the reflectance measurements, "% R". Baseline was set from "no baseline correction" to "100 % Transmission correction". Lastly, "UMA" was used to choose the angles that were being investigated, every tenth angle from 10° to 80° and the polarization. The measurements where first done with unpolarized light, then with p polarization and lastly with s polarization. The polarization order was chosen with no intention other than how it was set up in the program.

A blank measurement was first done prior to the measurements of the samples. The blank measurement was done as a 100 % transmittance baseline correction in order to minimize any measurement errors occurring in the grating/detector change in the Cary. The blank measurement had no samples mounted and the detector was automatically set 180° with respect to the light source. Without the baseline correction, the measurements created notches in the detector/grating change and were not usable for further investigation. The notches were not completely removed, but the measurements became much smoother after the baseline correction was done.

As the angle of incident of the light was increased, a larger area of the sample

was hit. To be certain that the light was fully measured, a 'zero order' beam was used before starting the measurement program. Each sample was mounted in the center of the sample mount and the UMA was then driven first to a near-perpendicular angle, 10° for this study, and then driven to the highest desired angle, 80°, to check that the entire beam was kept inside the sample. The zero order beam was white light.

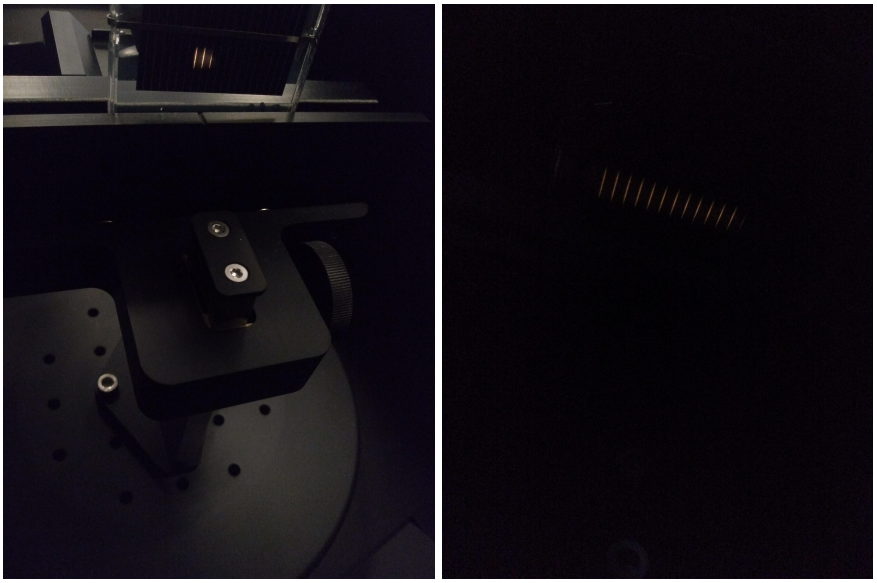

(a) Zero order beam for low angle (15°)

(b) Zero order beam for high angle (80°)

Figure 3.1: Use of the zero order beam show a clear increase in surface area as the angle of incident increased.

Fig 3.1 show how the zero order beam, and subsequently any other beam, have increased surface area as the angle of incident light is increased. Because of this area increase, the maximum angle of incident for the CNT sample had to be narrowed to 75° in order for the entire light to hit the sample. Every other sample was big enough to be measured from 10° to 80°.

3.2.2 Measurement Disturbances

It was early discovered in the measurement process that the widest parts of the interval(180 - 2800 nm) gave a large amount of disturbance in the measurements at both the longest and shortest wavelengths. Because of these fluctuactions at the ends, the measurement interval for the solar absorber measurements was narrowed down to 300 – 2500nm. Because of the irradiance pattern, see fig. 2.2, the narrowing had little to no impact..

During the measurements, two issues that continually occurred in turn altered the measurements differently for every individual sample in their individual measurement sequence, whether it was polarized or unpolarized. The first was a notch when grating and/or detector change occurred. Independent of the samples, the notch would be anything from negligible to be up to 3-4 percent. As described in the previous section, the notch was damped by the blank measurements. Without the blank measurements the notch could be as much as 15-16 percent, which would make the data unusable. The second measurement problem was measurement disturbance at the lowest wavelengths, in the UV region. As seen in the results, the disturbance caused alternating values of 1-2 percent above and below the "regular" measurements.

3.3 Reflectance Utilization

After the reflectance result was obtained it was used to calculated the absorbance for the best performing solar absorber. Unlike for solar cells, which has more variables and parameters which were not possible to acquire in order to calculate the efficiency, does eq. 2.3 calculate how much that is absorbed and ultimately gives the efficiency of the solar absorber.

With the measurements done for every tenth angle and the calculated absorbance for each of those angles, the angle dependent absorbance was found. With the angle dependent absorbance, the ability to insert in any desired angle(of interest) was possible. This was then used to map the absorbance for specific dates throughout the day, given that the incident angle was known. The ability to compare the absorbance between any two or more locations of the earth was possible. Eq. 2.16 was used to determine the angle of incidence throughout the day.

The angle dependent absorbance was also used to see how much of the irradiance of a specific day was absorbed. The irradiance data(W/m^2) was found using a censor on the roof of the Realfagsbygget(science building) at UiT. Knowing the elevation angle of the sun the specific day and the irradiance pattern of the sun, the absorbed power per unit area was calculated.

4

Results and Discussion

This chapter presents the results gathered from the reflectance measurements for the solar cell and solar absorbers. The results presented show the reflectance of unpolarized and p- and s polarized light. Each sample measurements are individually presented and discussed.

Reflected radiation, or albedo, yields different properties for light. One of which is that once the unpolarized light hit a surface, the reflected light often is partially polarized. At the higher latitudes in Norway and generally on the earth, the temperatures are low so the snow melts at a much slower rate than at lower latitudes. This gives rise to a strong reflection of light from the ground(snow in particular) for a long time over the course of a year, which can be utilized to solar energy.

In particular, two phrases were used throughout the result section. "Measurement Sequence" refers to the results from one specific angle, so each sample has eight measurement sequences. "Overall reflectance" refers to the entire, or a large portion of the, measurement curve in a measurement sequence.

Appendix A features the results not discussed in this section.

4.1 Unpolarized Results

4.1.1 Solar Cells

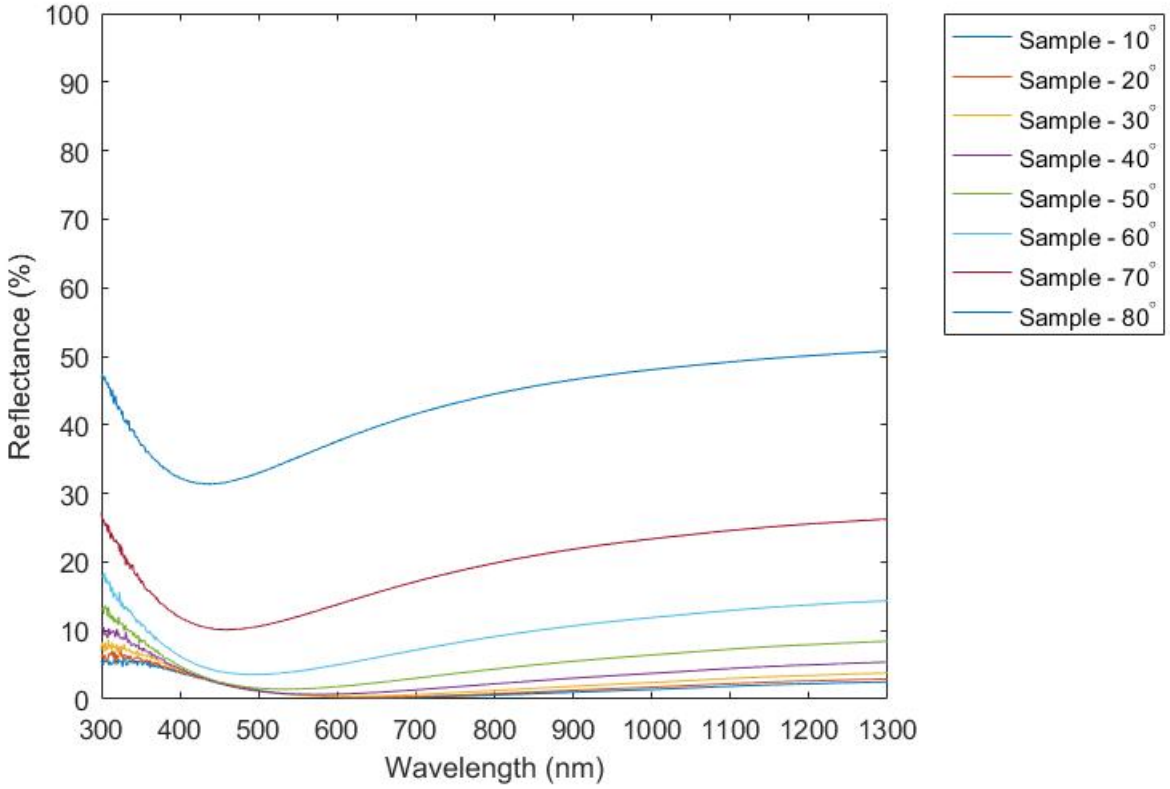

Figure 4.1: Reflectance measurements of the n-PERT 219 with EVA and 3.2 mm glass.

The n-PERT 219 reflectance measurements showed low reflectance on the entire measurement sequence for low angles.

For angles below 50° the reflectance was kept under 10% for the majority of the measurement sequence. For measurements at the lowest angles, the reflectance had a slight decrease in accordance with the wavelength decrease and ended with an increase in reflectance starting in the turquoise region(550-600nm). The measurements showed an almost negligible increase in reflectance between the $10 - 30°$ angles for all wavelengths, and the near-perpendicular angles show superb reflectance values of only a few percent. At the highest angles of incidence, the measurements showed higher reflectance for the longer wavelengths. From the long wavelengths, a significant decrease in reflectance occurs as the wavelengths became shorter. The measurement sequence has a minima in the 400-450 nm interval before a strong increase in reflectance

occurs at the shortest wavelengths.

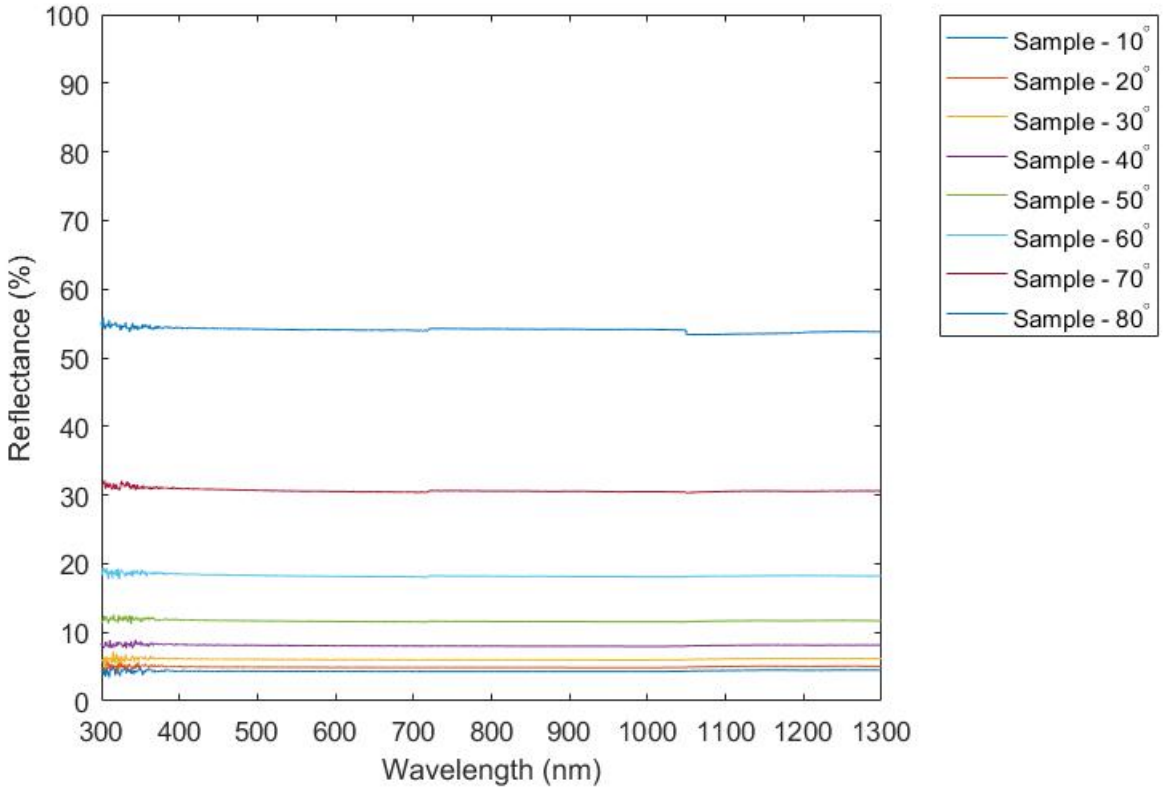

Figure 4.2: Reflectance measurements of the n-IBC1 sample, with EVA and 3.2 mm glass.

Fig 4.2 shows the reflectance measurements of the n-IBC1 solar cell sample. The measurements show approximately constant reflectance for the entirety of the measurement sequence. The reflectance has smaller increase between the measurement sequences at the lowest angles, and a more significant increase as the angle of incidence was increased.

The n-IBC1 sample showed the least expected curves of the solar cell samples. Together, the glass, EVA and cell, manages to keep the reflectance down to remarkable low values at the near-perpendicular angles. Since no one wavelength is preferable as they all contribute to excitation of electrons in the material, these results show promising results. It was expected to see an increase in overall reflectance as the angle of incident light was increased.

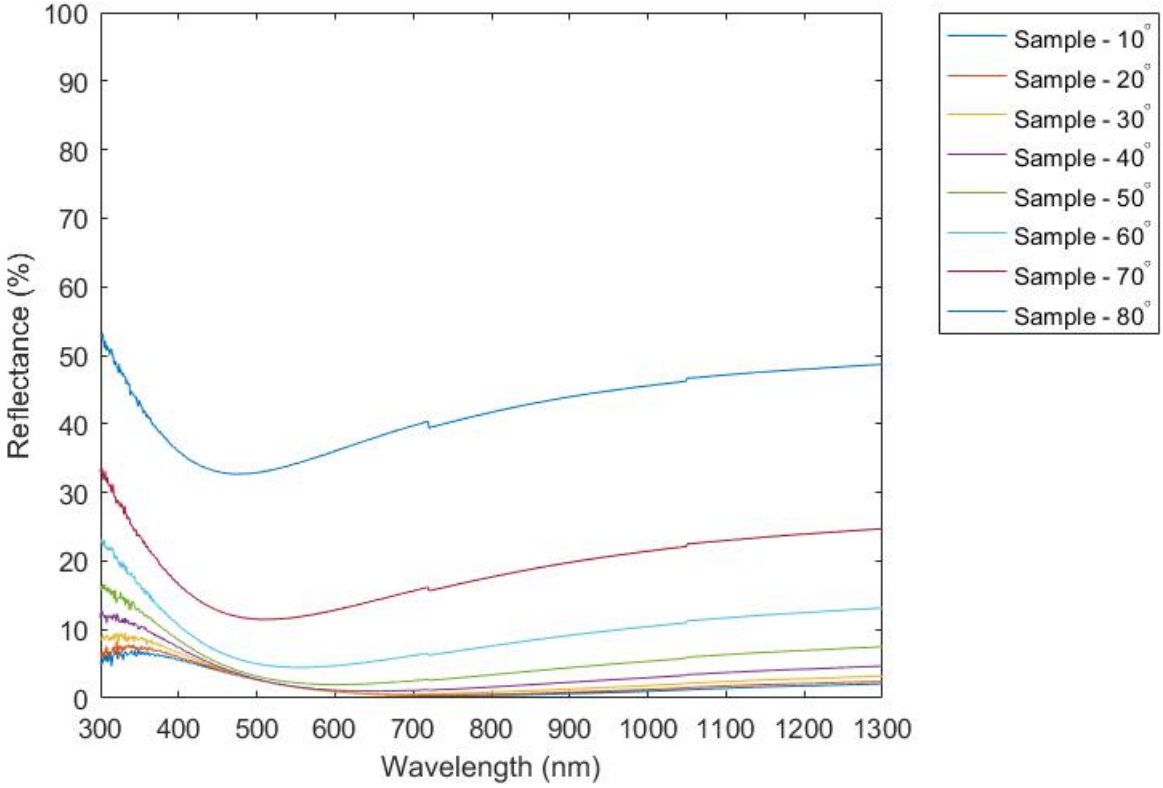

Figure 4.3: Reflectance measurements of the n-IBC 2 sample, with EVA, ARC and 3.2 mm glass.

The n-IBC2 measurements is shown in fig 4.3. With similarities to the n-PERT measurements, the reflectance is kept low for the majority of the measurement sequence with a slight increase occurring at 600 nm at the lowest angle. The results for the angles from 10° to 50° showed an overall reflectance under 10 % for the majority of the measurement sequences. At the shortest wavelengths, there is an increase in reflectance. As the incident angle of light was increased, the reflectance would start off higher at the longer wavelengths. At the highest incident angles, the reflectance decreased as the measurements kept going with a minima in the 400-450 nm wavelength interval.

The n-IBC 2 and the n-PERT 219 showed similaries in curve shapes. The n-IBC 2 samples had an ARC-glass which the n-IBC 1 did not have. The ARC is wavelength-specific and creates destructive interference for the desired wavelength. The destructive interference also causes an constructive interference and is the reason for the reflectance increase for the lowest wavelengths. The n-PERT solar cell has a passivation layer on top which effectively will work in similar fashion as the ARC-glass. Hence, the smiilarities between the n-IBC2

and n-PERT.

4.1.2 Solar Absorbers

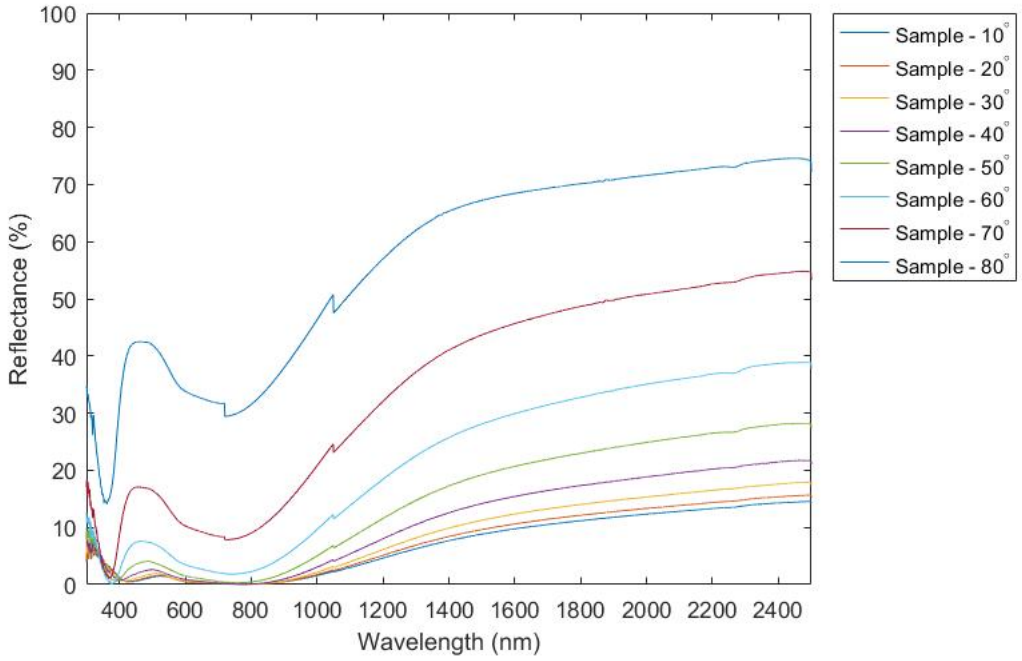

Figure 4.4: Reflectance measurement of the nickel-aluminum nanoparticle sample.

The selective surface of the Ni_xAl_x has almost zero reflectance in at near-perpendicular angle in most of the visible range. As the angle of incident was increased, the main difference in reflectance is noticable in the NIR range. The main concern for solar absorbers is to maintain a low reflectance in the visible range. This is where the majority of the irradiance from the sun is, and is the region the absorber mainly utilize to transform the solar energy to conduct heat. The Ni_xAl_x sample maintain low reflectance measurements up to 60°. For angle of incident light above 60° the reflectance has increased a significant amount for the whole measurement sequence.

The two declining curve slopes in the interval 300-1000nm, to a different degree for all measurement sequences, confirms that the solution-chemically absorber above consist of two layers. Each layer is created to cause destructive interference at the desired wavelenghts, preferably where the solar irradiance is high, when the light hit the surface. Similar to the effect in the n-IBC 2 solar cell sample, with the ARC-glass, the method of using destructive interference does also give rise to a constructive interference in the material. The constructive

interference is the cause of the reflectance increase around 500 nm. The second layer is used to counteract the constructive interference by creating a second destructive interference in the realm where there previously was constructive, to maintain a low reflectance in the desired wavelength interval, and subsequently another constructive interference occur at the shortest wavelengths.

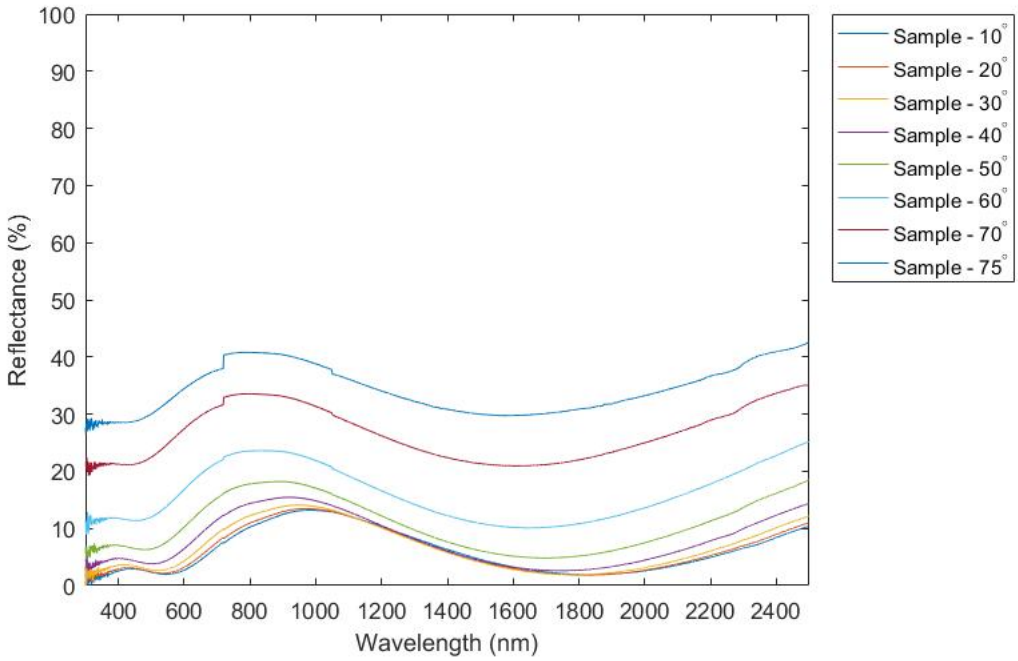

Figure 4.5: Reflectance measurement of the CNT structures.

For the CNT sample, the reflectance in the visible range was relatively high, compared to the other samples. As the angle of incident was increased, the overall reflectance also increase with a less pronouced increase in the red-region(1200-1700nm) of the visible range at lower angles. For measurement sequences higher than 50° there where no region that stood out with a more significant increase in reflectance. The overall reflectance increase was similar for all wavelengths.

From Fig 4.5, it seems that the reflectance increase slows down at the highest angles but that comes from the fact that the last angle increase in the measurement only was 5° because of samples size. The carbon nanotube structured surface showed a relatively poorer reflectance measurement than the nickel-aluminum structured surface.

The Alanod sample showed fluctuations in the reflectance measurements in the NIR range and a continual decrease in reflectance from approximately

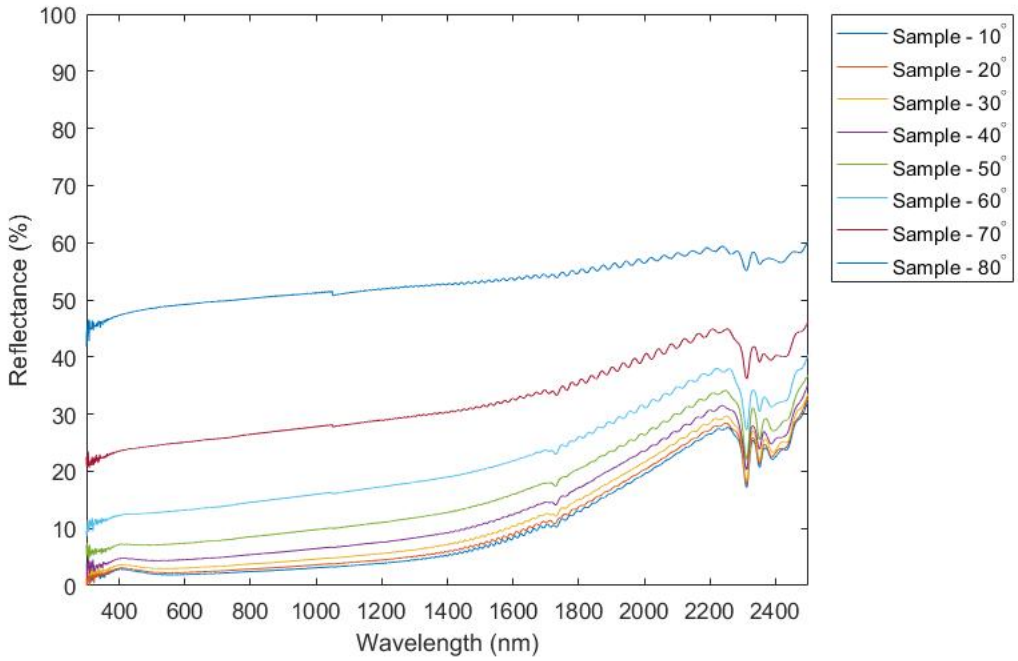

Figure 4.6: Reflectance measurement of the Alanod sample.

2300 nm to 400 nm. For lower angles, the reflectance had a slight increase for around 400nm, while at the higher angles there were a further decrease until the measurement sequence ended. In the visible range, the reflectance was measured under 10 % for angles up to 50°. The three last measurement sequences showed a significant increase in overall reflectance, especially in the visible range.

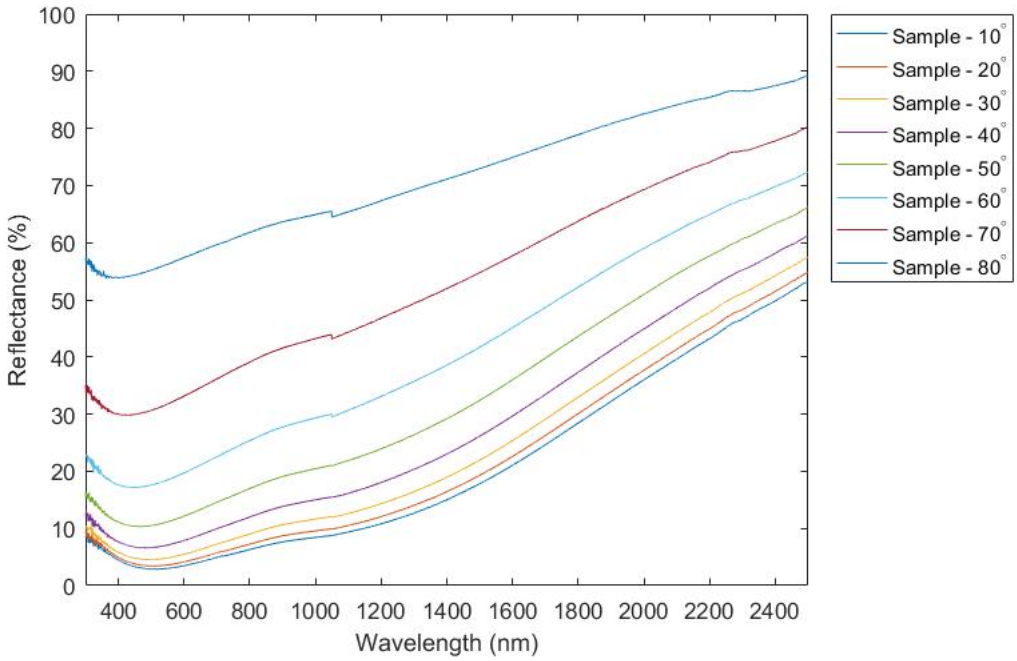

Figure 4.7: Reflectance measurement of the Sunstrip1 sample.

The SunStrip1 samples showed a generally a very high reflectance in the NIR range and a continuous reflectance decrease as the measurement sequence went on. As the angle of incident light was increased, a gradual overall increase in reflectance was shown from near-perpendicular angles to the higher angles. The reflectance start off higher for longer wavelengths and the drop was less pronounced and the reflectance remained higher. For 70° and 80° the drop is very small, giving an very high overall reflectance.

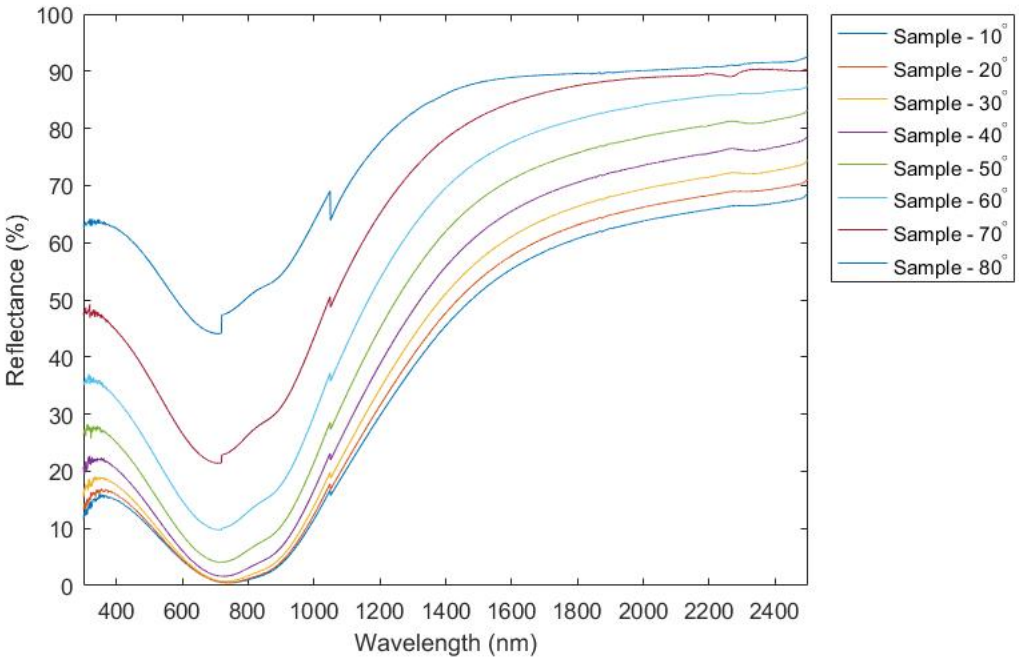

Figure 4.8: Reflectance measurement of the Sunstrip2 sample.

Fig 4.8 show the reflectance measurements of the SunStrip2 sample. It show the highest reflectance in the NIR range for all angles compared to the other samples, and has the steepest curve in the region switching from high to low reflectance in the red region of the visible range. For the shortest wavelengths, 300 – 700nm, the reflectance start to increase. The same structure occurs for all measurement sequences but as the angle is increased the slope of the reflectance curve occurring in the red region is shorter, giving an higher overall reflectance as the angle increase.

The measurements of the SunStrip2 sample show an earlier and steeper reflectance increase in the turqouise-blue region of the visible range than the SunStrip1 sample which has a continual decrease in reflectance until 400 nm where a slight increase occurs. With this in mind, an excepted results would be a significantly clearer blue colour on the SunStrip2 sample than for the SunStrip1 sample.

4.2 Polarized Results

For the measurements done with p polarized light, the results did generally show lower reflectance values. In order to make the figures more presentable, the y-axis has been narrowed down in size.

4.2.1 Solar Cells

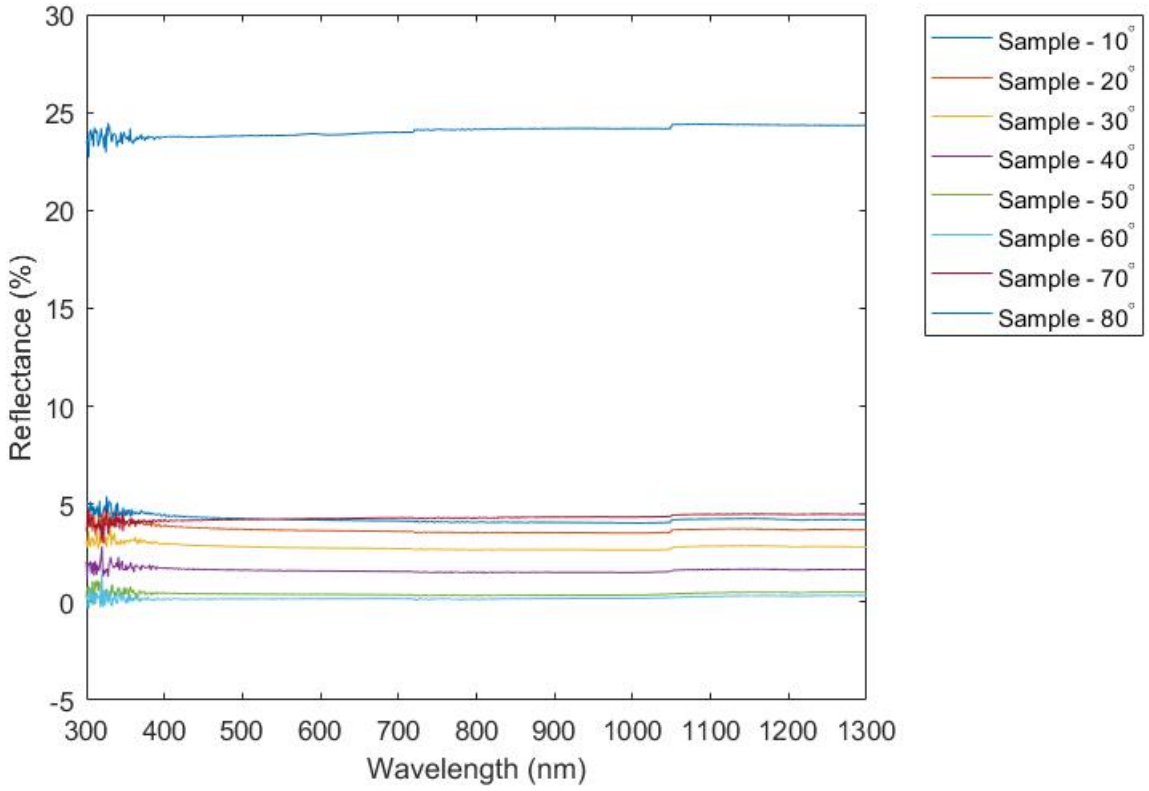

Figure 4.9: Reflectance measurements of the IBC1 sample with p polarized light.

The reflectance measurements of the n-IBC1 samples with p polarized light is presented in fig 4.9. At near-perpendicular incident angle the reflectance was measured right below 5%. As the angle of incident light was increased, the measurements showed a decrease in reflectance. The decrease continued as the angle of incident was increased to 60%. For the last two measurements the reflectance increased, with a overall difference of the meausurement were similar to the unpolarized measurements. Percentage increase in reflectance was $\approx$ 20% from 70° to 80° for unpolarized and p polarized measurement.

For the solar cell samples, as mentioned in section 3.1.1, standard glass was used as glass cover. The refractive index of glass is 1.52 while for air is approximately 1. The polarization angle between standard glass and air is thus,

$$\Theta_B = arctan(\frac{n_{glass}}{n_{air}}) \approx arctan(1.52) \approx 56.7^\circ \tag{4.1}$$

Observing the results with p polarized light from Fig 4.9, the measurements with incident angle of 60° showed the lowest reflectance results. This is in good accordance with the theoretical result that comes from the Fresnel equations for p polarized light(Eq. 2.10). The reflection coefficients, with the refractive indices given above, are presented below:

Table 4.1: Reflection coefficient of air-glass interface calculated from the Fresnel equation for p polarization.

Angle(°)	10	20	30	40	50	60	70	80
R_p	0.0659	0.0486	0.0327	0.0170	0.0038	0.0014	0.0340	0.1721

As the Fresnel equation for p polarized light suggests, the measurements should show a very low reflectance value and decline as the angle of incidence is shifted from near-perpendicular angle towards the polarization angle,Θ_B. A significant increase in reflectance occurs after the polarization angle is passed.

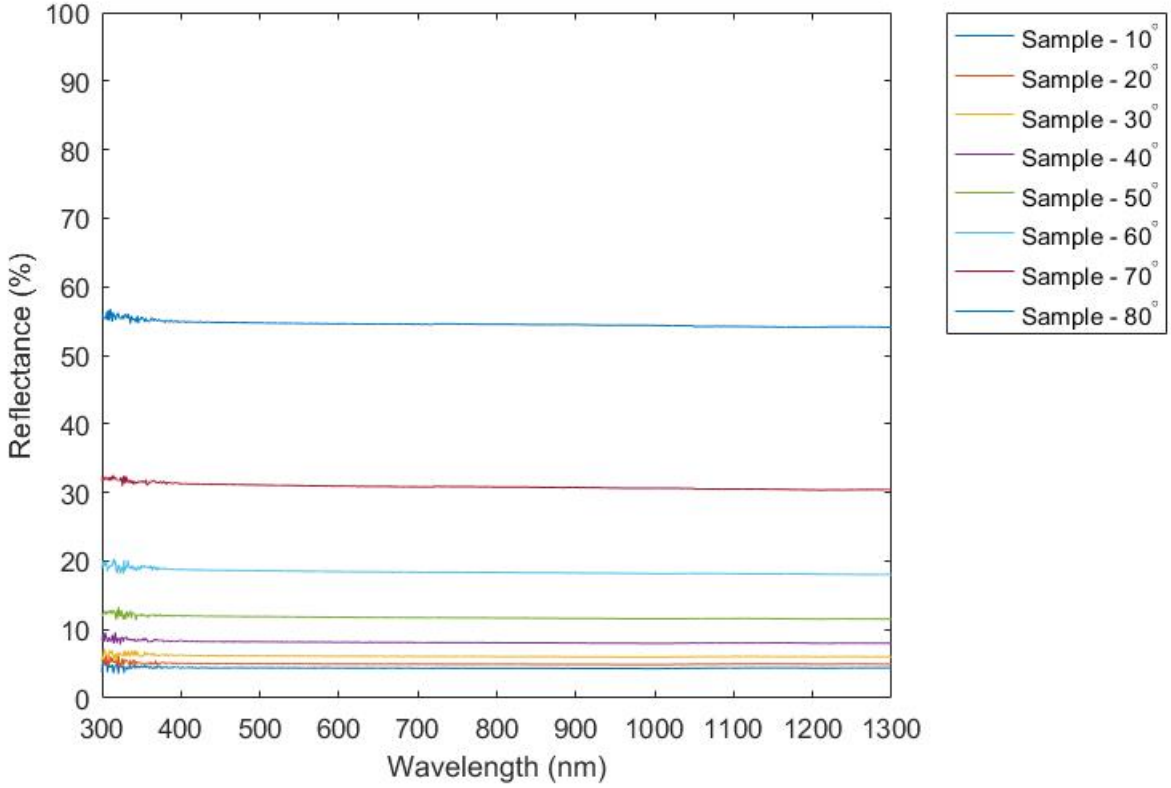

Figure 4.10: Reflectance measurements of the IBC1 sample with s polarized light.

Fig 4.10 show the reflectance measurements of the n-IBC1 sample with s polarized light. The measurements with s polarized light produced almost identical results to the unpolarized measurements, both in shape and angle-dependencies. For near-perpendicular angle, the measurements showed low reflectance values with slight increase as the angle of incident as increased. For higher angles, the measurement showed greater increase in the overall reflectance.

From the Fresnel equation for s polarized light, the reflection coefficients are

Table 4.2: Reflection coefficient of air-glass interface calculated from the Fresnel equation for s polarization.

Angle(°)	10	20	30	40	50	60	70	80
R_p	0.0443	0.0500	0.0612	0.0814	0.1174	0.1834	0.3079	0.5464

Unlike the reflection coefficients from the p-polarized light, where the coefficients show a gradual decrease in reflectance towards the polarization angle and then a sudden increase, the reflection coefficients of s polarized light show a continual increase as the angle of incident is increased. The reflectance measurements of the s polarized light and the numerical reflection coefficients show good concurrence.

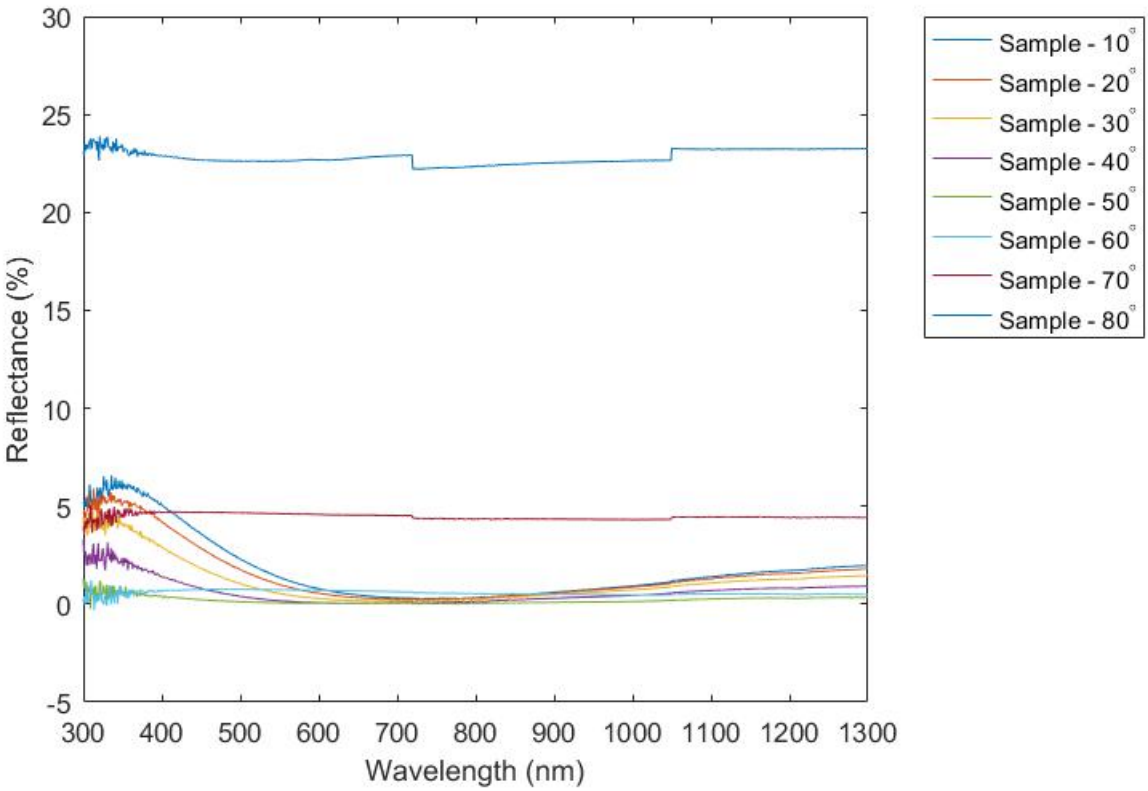

Figure 4.11: Reflectance measurements of the IBC2 sample with p polarized light.

Fig 4.11 show the reflectance measurements for the IBC2 sample with p polarized light. Same as the unpolarized measurements, the p polarized measurements show a different curvature for the sample with the ARC-glass, at the lowest angles. The same overall reflectance decrease appear in the IBC2 measurements, similarily to the IBC1 measurement. The lowest incident angle has a reflectance that start at approximately 2.5 % and has a decrease as the wavelengths get shorter, with a minima between 700-800 nm. The reflectance then has an increase towards the shortest wavelengths and end up at $\approx$ 5%. As the angle of incidence is increased, the overall reflectance measurement decrease on the whole wavelength interval and shows best performance at 50° with a average reflectance under 1%, see green line.

Once the angle of incident has past the 50° measurement sequence, the reflectance show a constant reflectance at the highest angles(the two notches at 700nm and 1050nm are due to the grating/detector change). These shapes of the reflectance measurements are very similar to the IBC1 measurements. The difference in overall reflectance increase show similar value as the difference between the reflection coefficients shown in table 4.1.

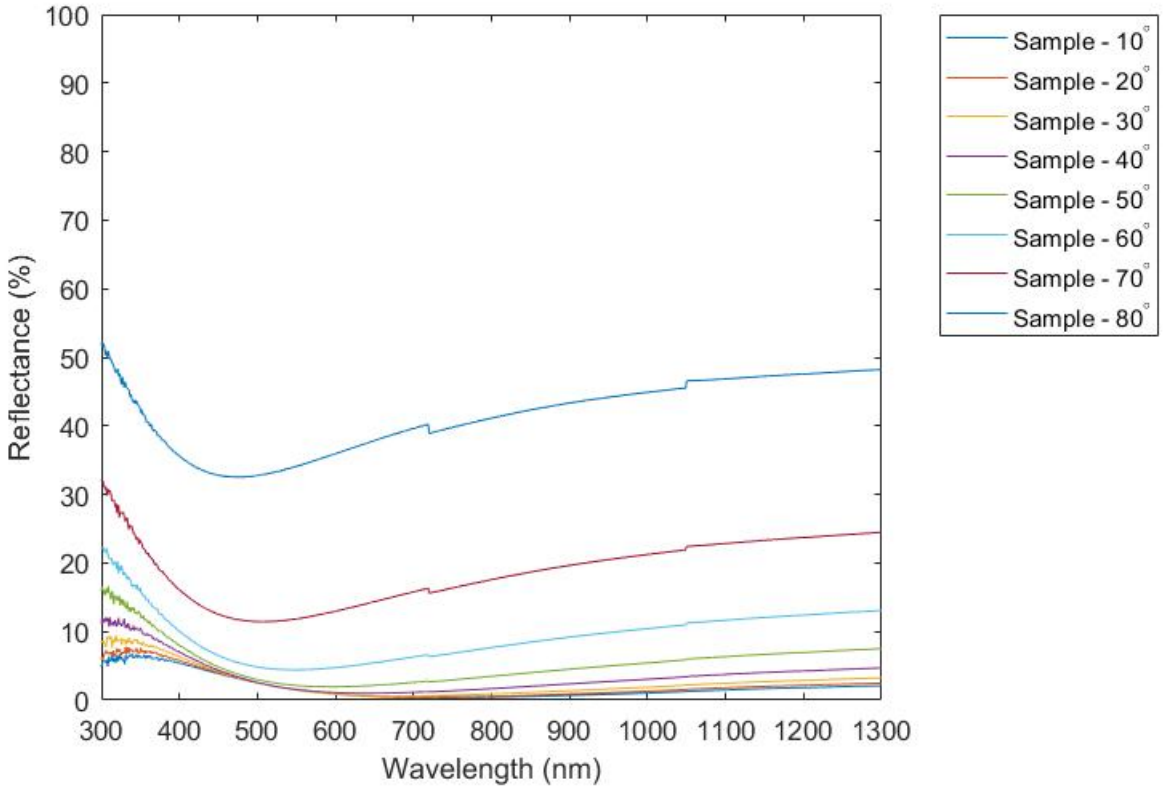

Figure 4.12: Reflectance measurements of the IBC2 sample with s polarized light.

The reflectance measurements of the IBC2 sample with s polarized light show the same tendencies as the IBC1 s polarized measurements. The measurements of with s polarized light are almost identical to the measurements done with unpolarized light. The difference in the measurements between the unpolarized and the s polarized is that the overall reflectance of the unpolarized measurements is very slightly higher than the s polarized results.

4.2.2 Solar Absorbers

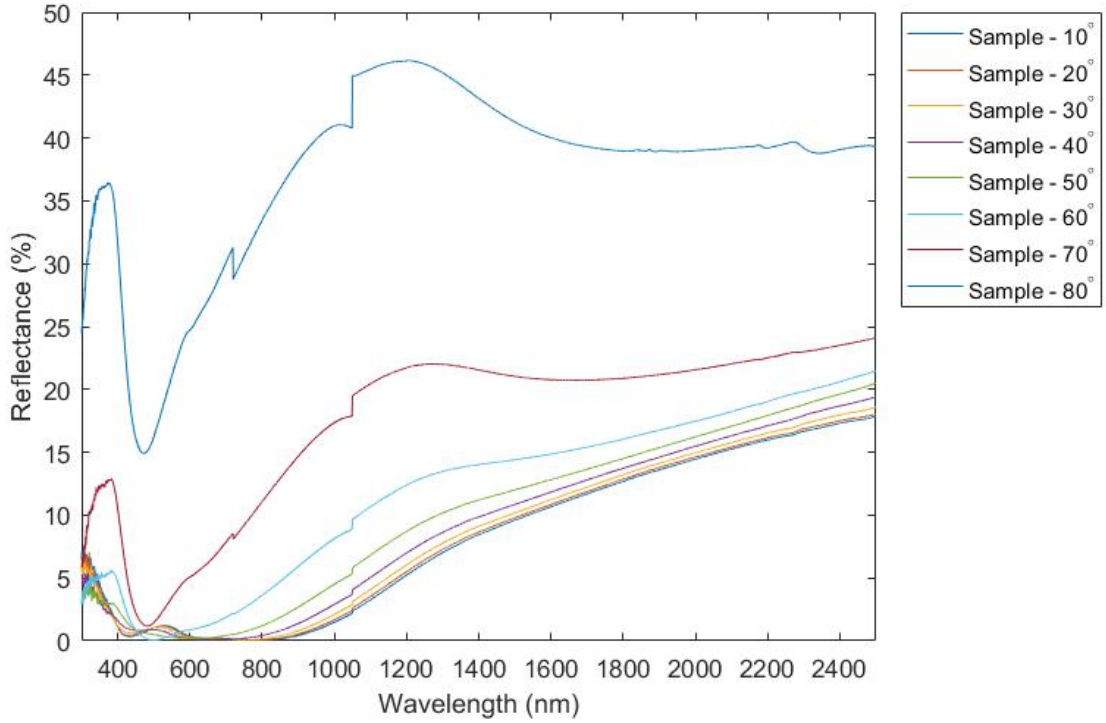

Figure 4.13: Reflectance measurements of the Ni_xAl_x sample for p polarized light.

At lower angles, the reflectance started off between $15 - 20°$, with a decreasing reflectance. The decrease continued to approximately zero reflectance in the red/orange region of the visible range. The reflectance had a slight increase in the turqouise region(500-550nm) and a significant increase in the shortest VIS- and UV range. When the angle of incidence was increase, similar pattern appeared for the lowest angles. At the highest angles, the measurements showed substantial overall reflectane increase. In difference with the unpolarized measurements, as the angle of incidence was increased the overall reflectance increase was lower for the p polarized measurements.

The reflectance measurements of the Ni_xAl_x with p polarized light showed different results than the solar cells. The results showed a gradual increase in the overall reflectance for all measurement sequences as the angle of incidence was increased.

Using the Fresnel equations for numerical confirmation is not as accurate for the solar absorbers, since the measurements has more curves and are not constant like the n-IBC1 sample. Nevertheless, the Fresnel equations give a pin-point on

how the different measurement should be relative to each other.

Table 4.3: Reflection coefficient of air-sample interface calculated from the Fresnel equation for p polarization.

Angle(°)	10	20	30	40	50	60	70	80
R_p	0.2033	0.1664	0.1295	0.0888	0.0453	0.0080	0.0103	0.1793

For numerical analysis the refractive index was set to $n_2 = 2\,17$. The refractive index is based off of the knowledge obtained from the unpolarized results(the reflectance curvature and the conclusion that it is two layered) and [Boström, 2006], the thesis where the sample originates from. From the numerical data of the Fresnel equations, the expected results should be an overall decrease in reflectance with the lowest reflectance measurement when the angle of incident was 60° and an increase at the highest angles. Instead, as it looks from fig 4.13, the overall reflectance from all measurement sequences seem to increase rather than decrease.

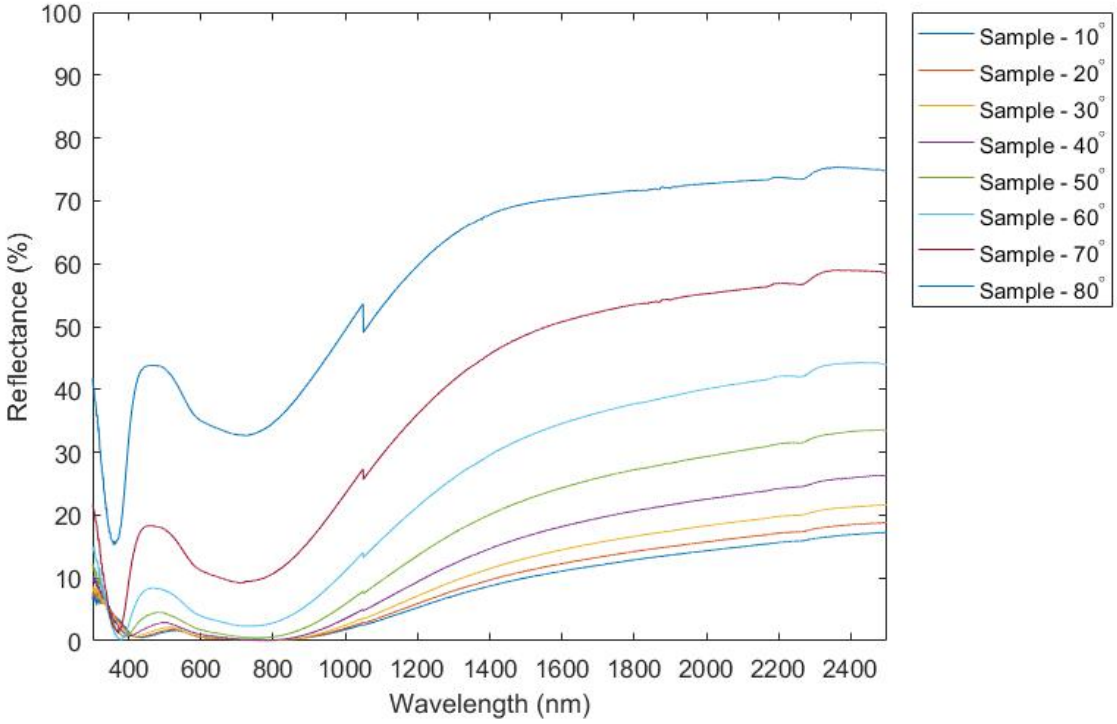

Figure 4.14: Reflectance measurements of the Ni_xAl_x sample for s polarized light.

The reflectance measurements of the Ni_xAl_x sample with s polarized light show great similarities to the unpolarized measurements. At the longest wavelength, the reflectance is a few percent higher in the s polarized measurements, but the overall curve is the same. The reflectance decrease as the wavelengths become shorter, with approximately zero reflectance in the red/orange region of the visible range. Then, a small increase in reflectance occurs in the turquise/blue region. As the angle of incidence is increased the shape of the curve remained the same, but show a slightly higher overall reflectance for the s polarized measurements.

Table 4.4: Reflection coefficient of air-sample interface calculated from the Fresnel equation for s polarization.

Angle(°)	10	20	30	40	50	60	70	80
R_p	0.1401	0.1523	0.1750	0.2119	0.2694	0.3580	0.4933	0.6975

The measurements show a similar overall reflectance increase as the reflection coefficients does.

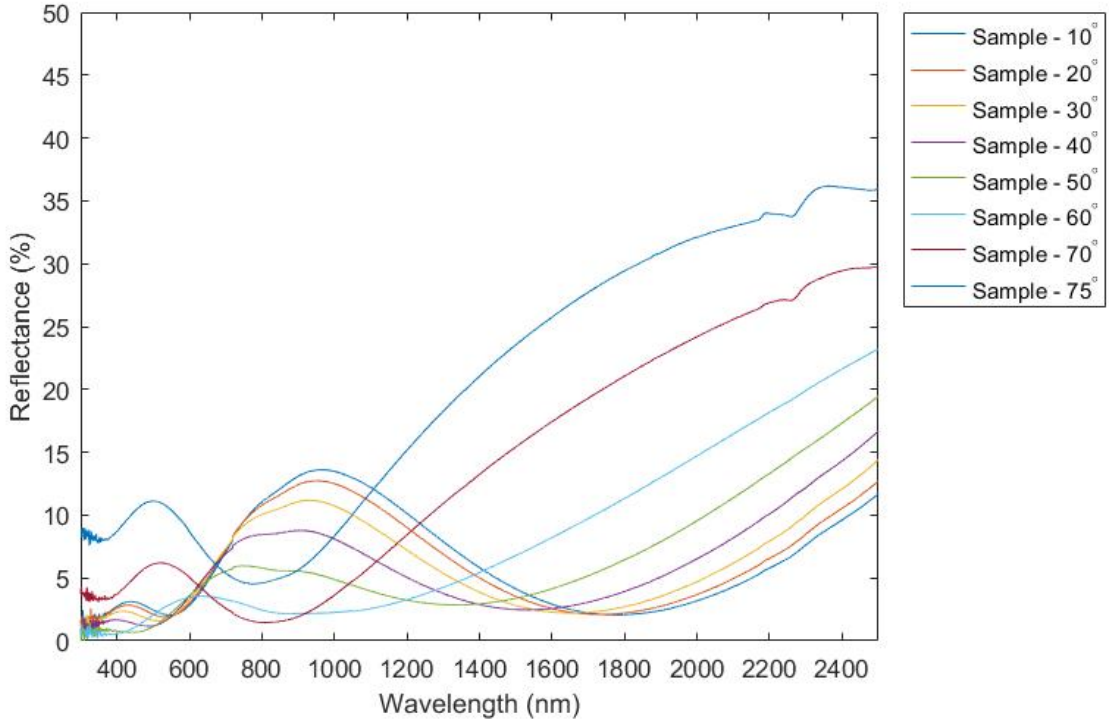

Figure 4.15: Reflectance measurements of the CNT sample for p polarized light.

The reflectance measurements of the CNT sample with p polarized light is presented in fig 4.15. At the first measurement sequence the measurement started at ≈ 12%, with a decrease in reflectance until 1800nm. The reflectance then showed an increase from ≈ 1800nm to 900 – 950nm, with a peak reflectance of ≈ 14%. Lastly, a second decrease occurred, to 1 – 2% reflectance in the blue region(500 nm).

As the angle of incidence of light increased, the measurements showed higher reflectance for the longest wavelengths(1800-2500 nm). Similar to the first measurement sequence, the reflectance increase occurred at shorter wavelengths accordingly to the increase in incident angle. The slope between ≈ 500 – 1800nm became shorter and smaller, showing higher efficiency at higher angles(20 % - 50 %). At the 60° measurement sequence, the reflectance was higher for longer wavelengths but on the wavelength interval 300-1000 nm it showed very low reflectance values, never exceeding 5 %.

The two last measurements showed a slower reflectance decrease towards the visible range. Unlike the first measurement sequences, which had an increase in the red region of the visible range, the last measurements had the lowest reflectance in the same region. Then, an increase occurred for the shortest

wavelengths, in the blue and UV region.

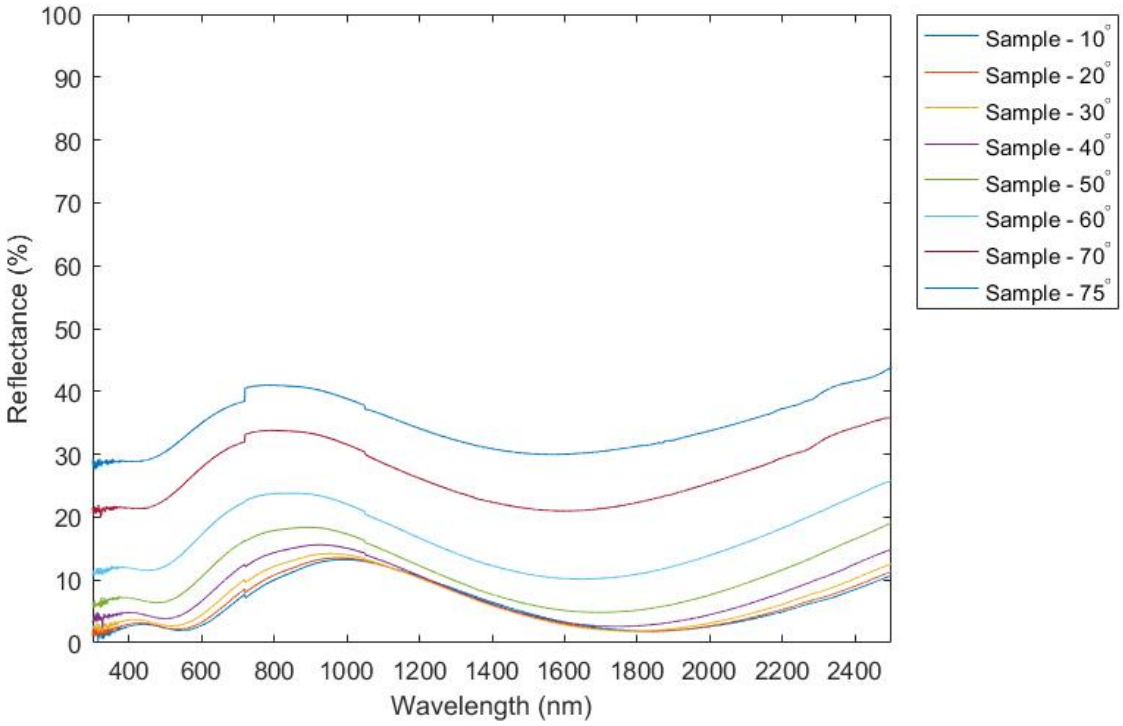

Figure 4.16: Reflectance measurements of the CNT sample for s polarized light.

The reflectance measurements of the CNT sample with s polarized light is presented above. Fig 4.16 show the same pattern for the reflectance measurements of s polarized light as earlier. For the CNT sample an almost identical measurement as the unpolarized measurement with decrease in the NIR range, an increase in the NIR-red range of the visible range and lastly a decrease in the turquoise/blue region.

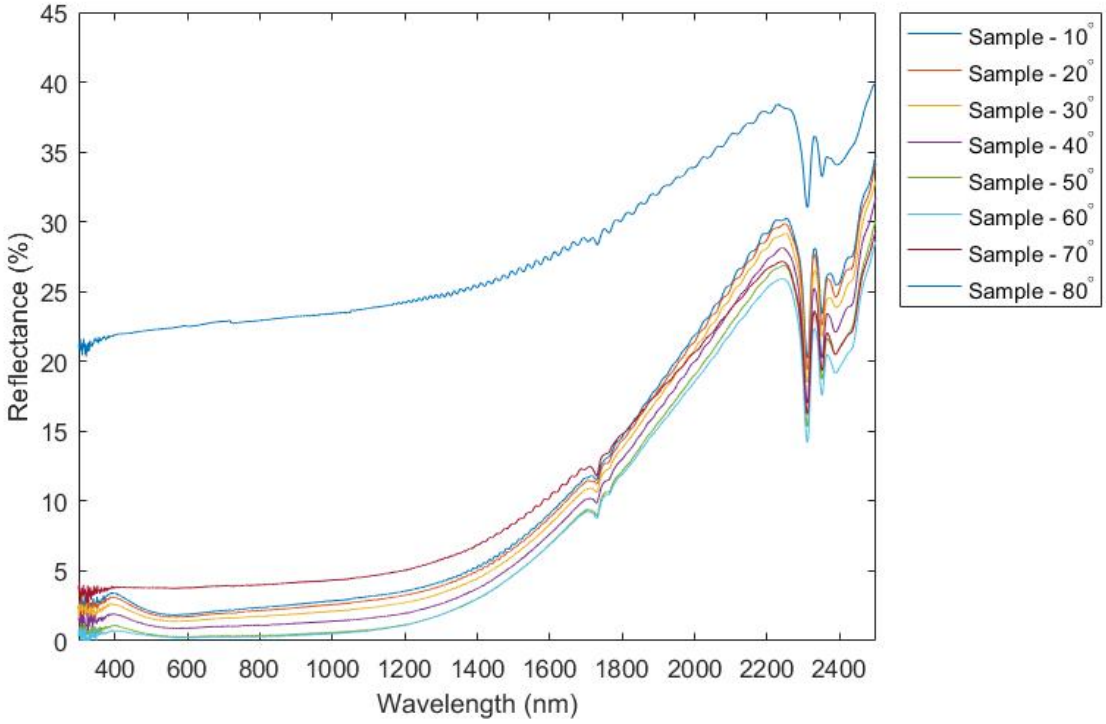

Figure 4.17: Reflectance measurements of the Alanod sample for p polarized light.

The reflectance measurement of the Alanod sample with p polarized light show overall decrease in reflectance from the near-perpendicular angle to the 60° measurement sequence, which show the lowest reflectance relative to the wavelengths, on the entire measurement sequence. The measurements with p polarized light show similar fluctuations in reflectance at the longest wavelengths as the unpolarized measurements. As the measurement sequence got to the 2200 nm, the reflectance decrease became more stable. For all measurement sequences, except for the last with the highest angle of incidence, the reflectance was measured under 5 % between approximately 300nm and 1200nm. The measurement with the two highest angles of incidence, 70° and 80°, show an overall increase in reflectance from the 60° measurement, with a substantial increase for the last measurement.

The reflectance measurement of the Alanod sample with s polarized light showed clear similarities to the unpolarized measurement.

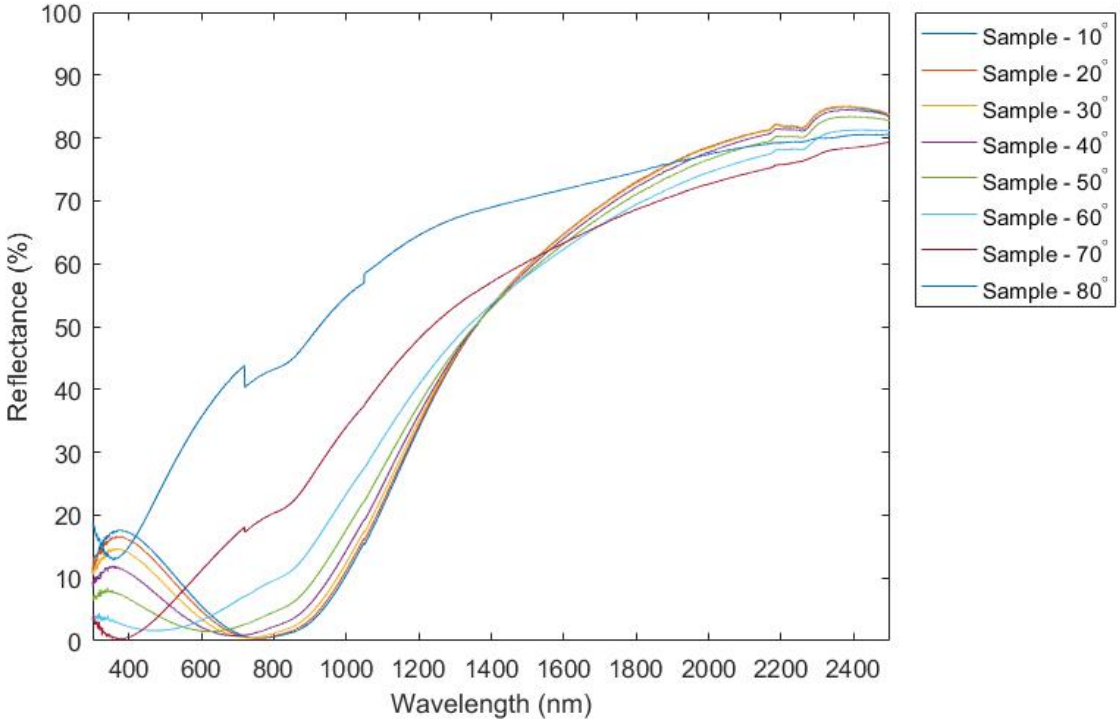

Figure 4.18: Reflectance measurements of the SunStrip2 sample for p polarized light.

Presented in fig 4.18 is the reflectance measurement of the SunStrip2 sample with p polarized light. It shows that at near-perpendicular angle of incidence, the reflectance is highest at the wavelength interval 1400-2500nm. On the interval 700-1400nm, the reflectance is lowest for the measurement sequences with the lowest angle of incidence and then lastly, from 300-700nm, the measurements showed a higher reflectance at near-perpendicular angle of incidence than the angles of incidence that tend to have a lower reflection coefficient from the Fresnel equations. Although the reflectance at the longer wavelengths was lower for the measurements with the highest angle of incidence, the measurements showed a substantially higher reflectance in the UV-VIS-NIR range.

4.2.3 Remark - Refractive indices and Reflection Coefficients

Apparent for the reader, the refractive indices and the reflection coefficients were only mentioned a few times during the discussion of some results. The refractive indices of the samples were not explicitly given for any of the samples, so the refractive indices given above are purely based on what I could find myself.

4.3 Quantification

The reflectance measurements alone will give the answer to the question, "What amount of light will be reflected off this surface at this given wavelength?". The question in itself is not bad, but it will probably not provide enough substance or weight. Two small comparison studies are therefore presented in this section. Both use the results from the best performing solar absorber sample(The Ni_xAl_x sample).

The first study compare how the elevation angle of the sun change over the course of three different date in the year, 15th of april, 15th of june and 15th of september, in Tromsø and a city significantly closer to the equator to see the impact of the change in incident angle for a city in the higher latitudes and a city which is generally presented as a "better" place for utilizing the sun as a energy source. The comparison will provide an insight to how the latitudinal differences affects the solar absorber. The reasoning behind the dates was to chose dates that covers alot of ground with just a few dates. These three dates gives the solar position throughout the day in spring, summer and autumn.

The second study use irradiance data provided from SolarEdge Technologies, with a censor located on the roof of Realfagsbygget(science building) at UiT [Solar Edge, 2018]. The study addresses one day in 2018 close to a date used in the first study, 17th of april, where the solar irradiance was relatively high and compares how much direct irradiance it is that day and how much that would be absorbed using the Ni_xAl_x sample as solar absorbers.

4.3.1 Absorbance of Solar Absorber Sample

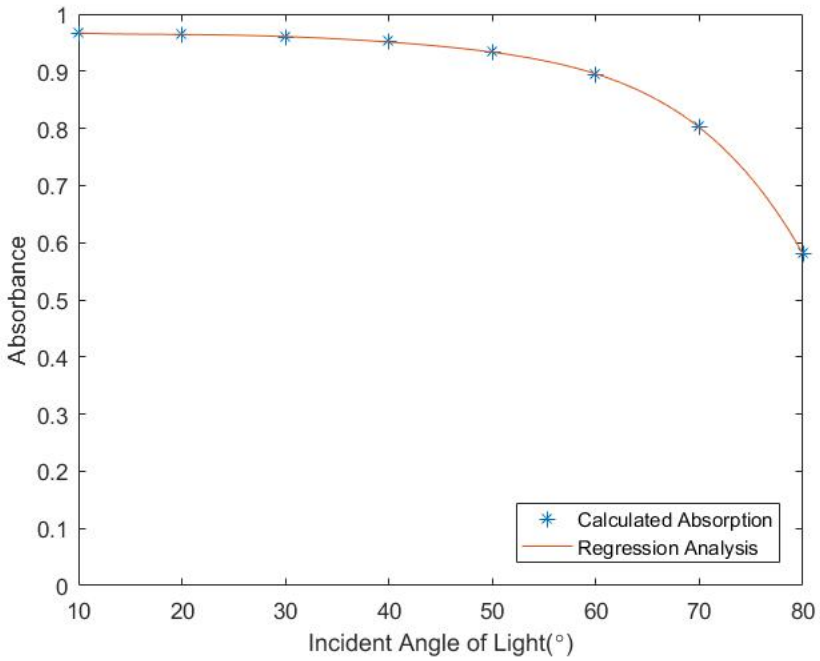

Figure 4.19: The angle-dependent absorbance of the Ni_xAl_x sample.

The angle-dependent absorbance of the best performing solar absorber sample is presented above. The star points are the calculated normal solar absorption using eq. 2.3 and the reflectance results presented in Fig 4.4, and the curve is a regression of the absorbance. The regression was produced to be able to chose an arbitrary angle, which in turn is used in the comparison study below. Fig 4.19 show that the angle-increase has a smaller impact at the lower angles, and as the increase in angle continues above 40°, the absorbance start to decline at a higher rate. At the highest angles, the absorbance value fall rapidly.

The most fitting curve showed to be a fifth order polynomial. Fig 4.20 shows that a fifth order polynomial would give a satisfactory curve for further investigation. The second order deviate too much to be a viable option for the use in this quantification. The fourth order polynomial, at initial look, has a good shape but at lower angles there appears to be a slope that alter the natural curve between the points. When the 5th order polynomial was introduced the curve looked accurate enough for further investigation.

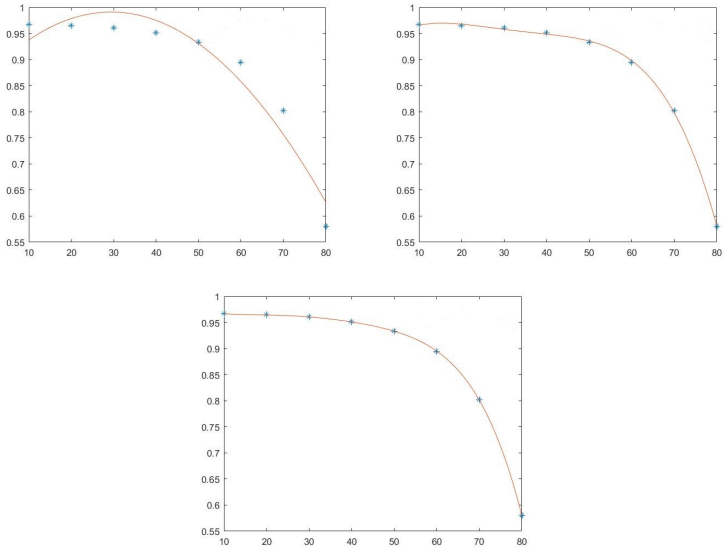

Figure 4.20: The 2nd(top left), 4th(top right) and 5th(bottom center) order polynomial of regression for the expression of absorbance.

4.3.2 Comparison Study: Absorbance in Tromsø and Rome

For the first comparison study it was necessary to find a source that could provide data on how the elevation angle of the sun changes in selected location on the earth throughout the day. Casio Computer Co. provides such services and their website was used during this study [Casio Computer, 2018]. The elevation angle of the sun was gathered for every fifteenth minute over the course of three different dates across the year, 15th of april, 15th of june and 15th of september. Using three different dates provide a more robust analysis as the amount of time the sun has an elevation angle > 0 changes for specific days.

The comparison was done for the absorbance of the solar absorber(set in two locations) and also for the incident angle of the sunlight on the solar absorber surface for both locations. Since the absorbance in this study is directly dependent on the incident angle, it is helpful to see how the absorbance and incident angle of light move in accordance with each other as the day progresses. For the comparison study, the solar absorber angle was set to 40° directly south in both Tromsø and Rome. The mounting specifications was chosen as it was because it is the same as the irradiance censor on the roof of Realfagsbygget.

For the following study does the blue curves represent the absorbance and the orange curves represent the incident angles of the sun. The solid curves

represent Tromsø, while the dashed represent Rome.

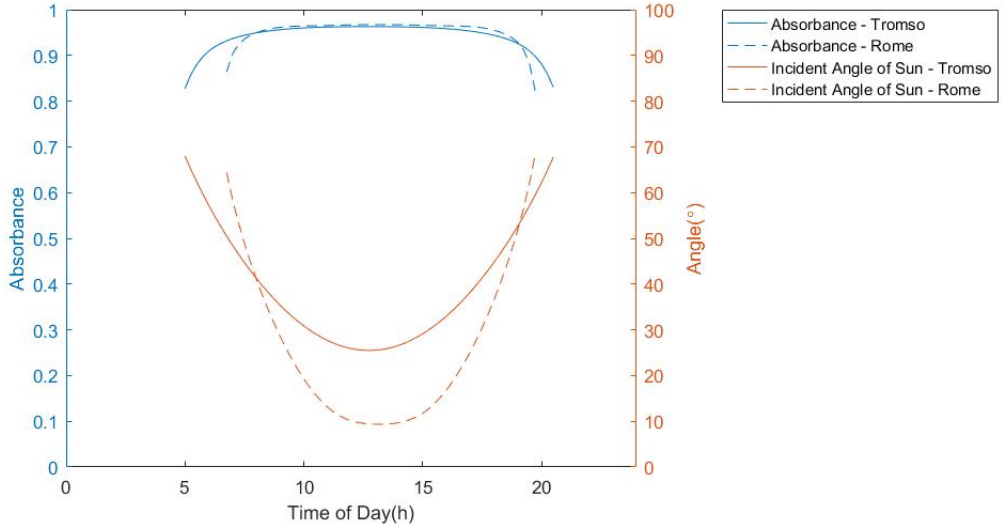

Figure 4.21: Absorbance and angle as a function of time on the fifteenth of april.

At the fifteenth of april, sunrise was approximately 05:00 in Tromsø while in Rome it was 06:45. Sunset was 20:30 in Tromsø and 19:45 in Rome. Even though the sun appears for longer in Tromsø than in Rome, the incident angle of the sunlight as it hit the solar absorber is more preferable in Rome. Fig 4.22 shows that the incident angle in Tromsø, for the majority of the day, is higher than in Rome giving a lower absorbance. Because of the angular orientation, the averaged absorbance in Rome is higher, μ_R = 95.2 %, than the average absorbance in Tromsø which is μ_T = 94.0 % for the fifteenth of april.

15th of june is part of the year where the midnight sun phenomenon occurs in Tromsø. As fig 4.22 suggests, the elevation angle in Tromsø is above zero all day. Unlike 15th of april, the incident angle is not so dominantly better in Rome than in Tromsø which is also reflected in the absorbance values. The absorbance is only better in Rome where the elevation angle crosses the perpendicular point of the solar absorber, which is around 09:45 and 15:15. The rest of the comparable time, then the sun is up both in Tromsø and Rome, the incident angle is set more preferable in Tromsø than Rome yielding a higher absorbance. the average absorbance on the 15th of june, for Rome and Tromsø respectively, is μ_{Rj} = 95.1 % and μ_{Tj} = 94.3 %. As this is an average across the entire time the sun appears, the average in Rome shows a higher average. The average taken from 05:45 to 20:45(the time period the sun appears in Rome), then μ_{Rj} stays the same but μ_{Tj} = 96.1 %, showing a greater absorbance in Tromsø than in Rome.

On the 15th of june is not only does the absorbance value higher in Tromsø than in Rome in the same time interval, the amount of time where the sun can

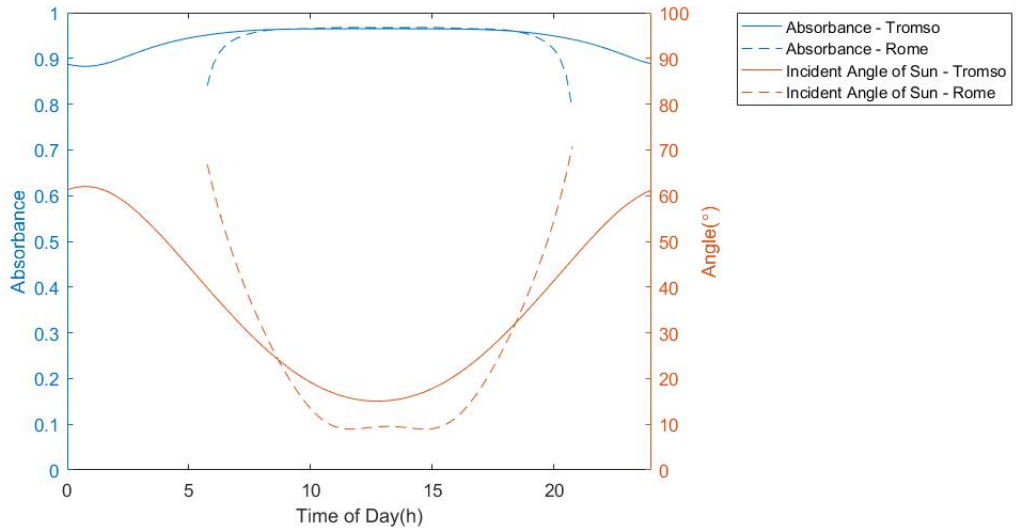

Figure 4.22: Absorbance and angle as a function of time on the fifteenth of june.

be utilized is significantly higher.

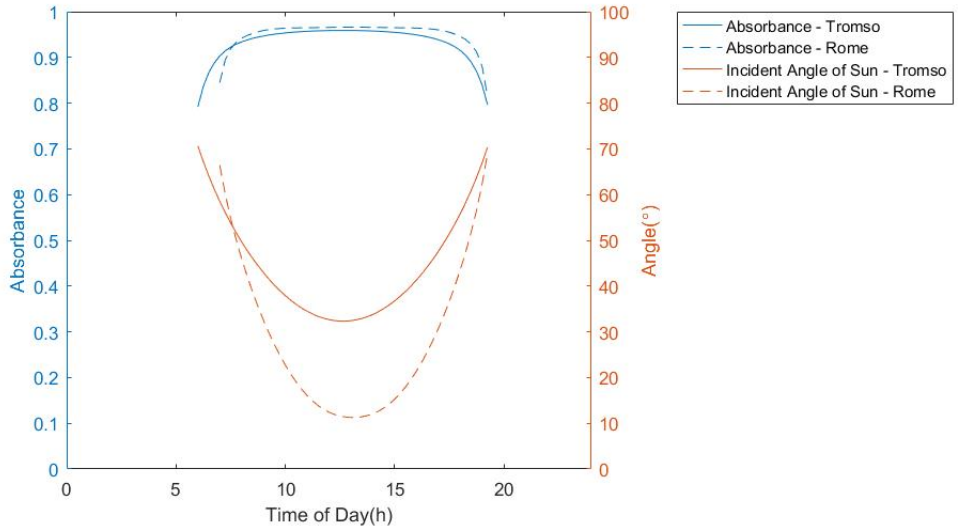

Figure 4.23: Absorbance and angle as a function of time on the fifteenth of september.

15th of september was the last date in the comparison study. From the incident angle curves, it is appearent that it is the date where the sun has its lowest elevation increase throughout the day. Because Tromsø is at higher latitudes than Rome, the elevation angle is significantly lower than in Rome which has a large impact on the overall absorbance. The average absorbance in Rome is

μ_{Rs} = 95.0 % and the average absorbance in Tromsø is μ_{Ts} = 93.1 %, the lowest average over the course of these three dates.

Study Remarks

The choice of angle for the solar absorber, 40°, was as mentioned earlier because of the mounted angle of the irradiance censor used in the next comparison. This is, with great confidence, not the optimal angle. As depicted, especially in the 15th april and 15th september plot, the optimal angle in Tromsø would be a higher angle to meet with the low elevation angle of the sun in the higher latitudes of the northern hemisphere. Arguable, the optimal in Tromsø would around 60°. This would provide a lower angle of incident for the light, which in turn would increase the absorbance as demonstrated in fig 4.19. For Rome, the chosen angle is much closer to the optimal angle. It can be recognised from fig 4.22-4.24 that the incident angle is generally closer to a perpendicular angle. The optimal angle for Rome is slightly lower than 40°.

Having a stationary mounted system does show to decrease the absorbance significantly for all dates. The absorbance does almost fall down to 80 % efficiency for all dates in Rome while on 15th of June in Tromsø, because of the midnight sun, manages to retain an absorbance of over 90 %. On the two dates, the absorbance in Tromsø does also come close to 80 % absorbance, an almost 15 % efficiency loss.

The comparison study shows that the solar absorber has a higher efficiency in the spring and autumn in Rome, while in summer the solar absorber has a higher efficiency compared to the operating time of the same absorber in Rome as well as a considerably longer operating time because of the midnight sun.

4.3.3 Comparison Study: Absorbance with Real-Time Irradiance Data

The second comparison study done in this thesis was to use the angle dependent absorbance as a function of the time of the day to investigate how the angle of incidence affect the absorbance of a solar absorber throughout one specific day of the year. The day chosen was 17th of april which was the closest date to 15th of april where the day had a large amount of solar irradiance in Tromsø. The censor used to collect the irradiance data was set at a 40° angled directly south.

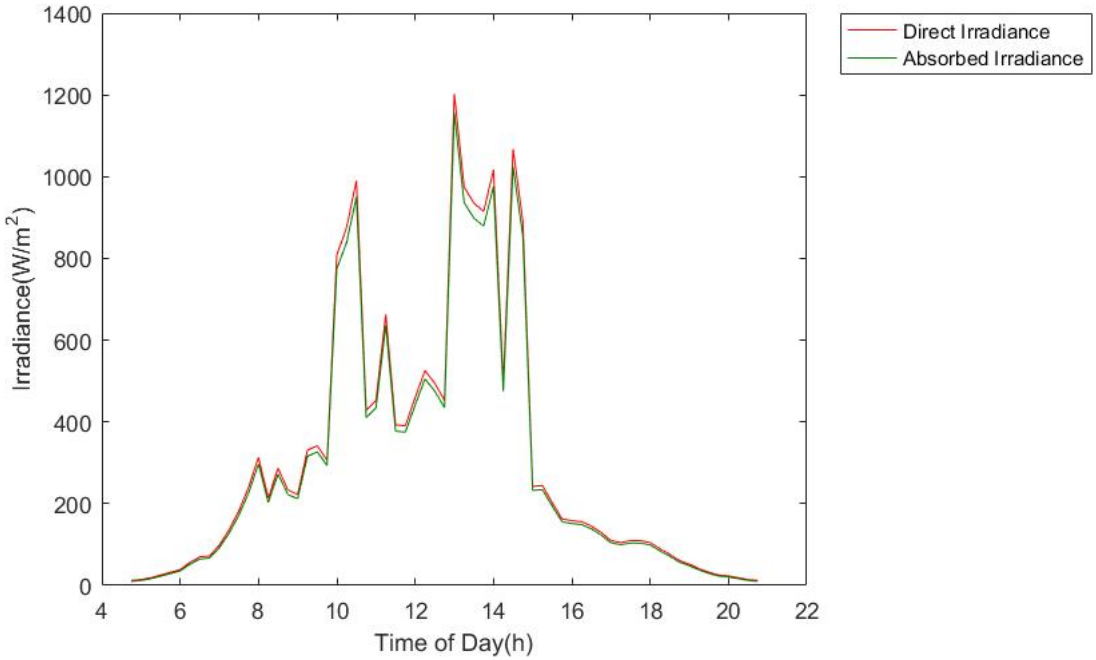

Figure 4.24: Plot of the direct irradiance(red) from the sun and the absorbed light of the solar absorber(green).

Fig 4.24 shows how the irradiance changed over the course of 17th april 2018(red line) throughout the day. The green line shows how much of the irradiance that was absorbed using the same angle-dependent absorbance regression like the previous comparison. In the plot there is an clear fall in irradiance between 10:30 and 13:00. This is most likely due to cloud formations in front of the sun and therefore causing a non-ideal situation, with less irradiance. The same goes for the period 7:45 to 9:45, where there is a gradual increase in irradiance and then a sudden stop in increase, before a step inclination occurs at approximately 9:45.

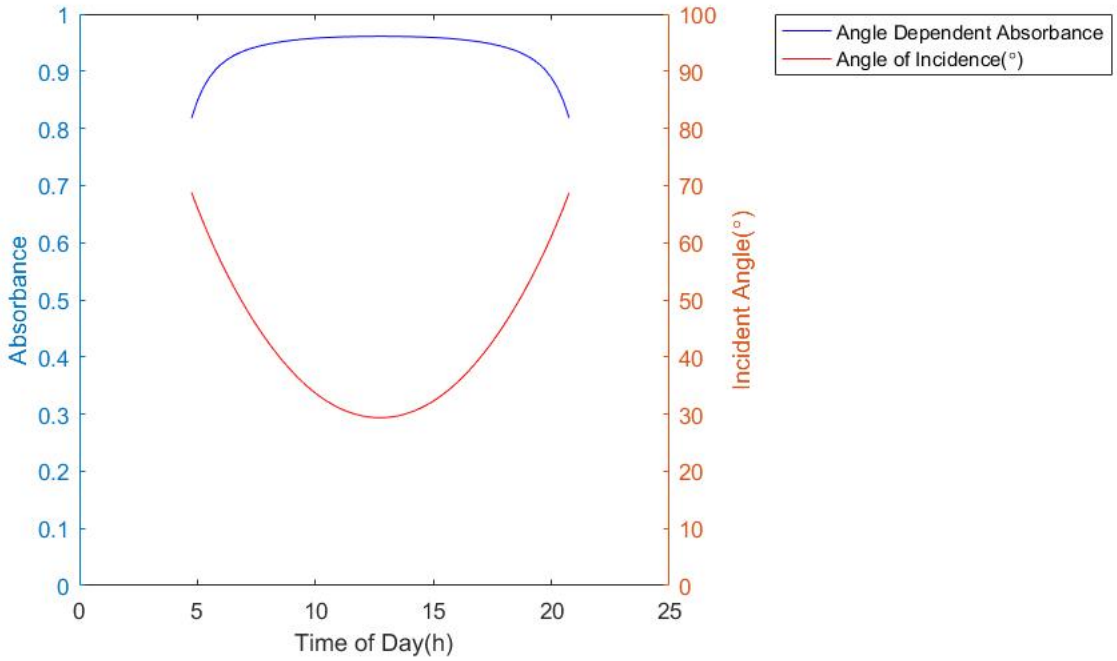

Figure 4.25: Plot of the incident angle and the absorbance throughout 17th of april.

From figure 4.25, it is apparent that the sun still is set low on the horizon and therefore the incident angle is high the entire day. Granted that the solar absorber has an average efficiency of $\approx 96\%$, the incident angle ultimately affects the performance of the solar absorber and the irradiance is not absorbed fully.

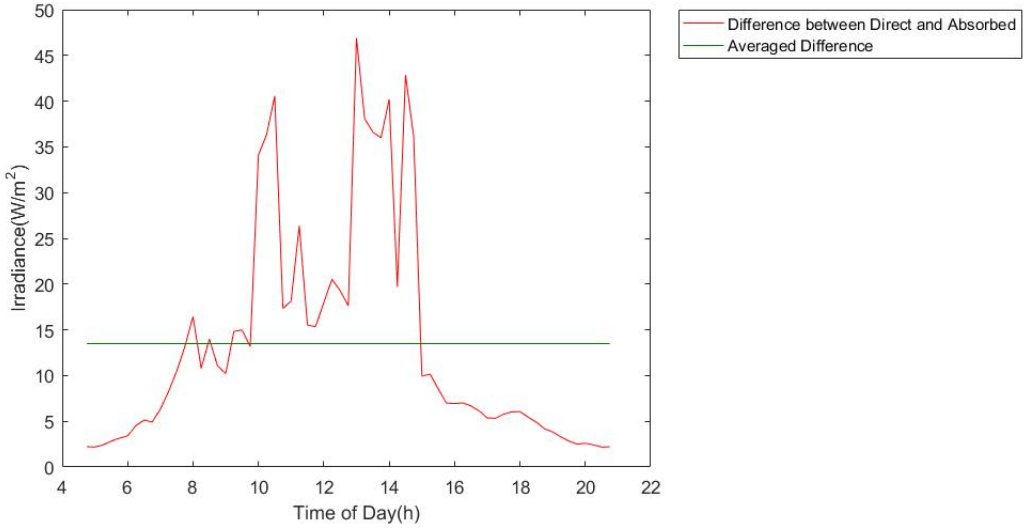

Figure 4.26: The difference between the direct and absorbed irradiance plotted with the daily average.

The difference between the direct and absorbed irradiance(red line) and the average across the day(11.6 W/m^2) is presented in fig 4.26. The figure shows that the largest difference in direct and absorbed irradiance is in the middle of the day. That comes from the fact that the solar intensity is higher and even though the incident angle is lower and subsequently the absorbance is higher, the loss will be more significant because of the magnitude of the irradiance.

Fig 4.26 shows that even on a day where the sun is set fairly low and early in the year, the losses due to the orientation of the module is substantial, especially in the morning and the evening. Pre and post mid day show that a lot of power is utilized poorly. The power loss can be reduced significantly if the module has a tracking system to orient the module during the day.

5

Conclusion

In this thesis, reflectance measurements with unpolarized and polarized light were done for a broad selection of angles with both solar cells and solar absorbers. The measurements showed that both the solar cells and solar absorbers respond well to small increase in incident angle of light, but as the angle of incidence became large the increase in reflectance became substantial, subsequently lowering the efficiency. For polarized light, the measurements produced results with good accordance with the reflection coefficients from the Fresnel equations for the solar cells. The p polarized light, the reflectance decreased as the angle of incidence was shifted towards the polarization angle. This include a minimum reflectance measurement for angles higher than near-perpendicular.

A comparison study was done, investigating how the angle dependent absorbance, calculated from the angle dependent reflectance measured earlier in the thesis, changed over the course of three different dates(15th of april, 15th of june and 15th of september) in a year in two different locations, Tromsø and Rome. During the study, a nickel aluminum based solar absorber was used. The study showed that the latitudinal differences between Tromsø and Rome had a small effect. The solar absorber performed better in Rome on the 15th of april and 15th of september, while the solar absorber performed better in Tromsø on the 15th of june.

Lastly, another comparison study was done. The Solar Edge monitoring system on the roof of realfagsbygget(science building) at UiT was used to gather the

irradiance data during one specific date, 17th of april. The same solar absorber as in the previous study was used to see how much of the incoming irradiance was absorbed by the solar absorber, theoretically. The study found a substantial loss of irradiance due to the decrease in absorbance as the day went, and found that the performance was poor pre and post mid day due to the stationary setting.

Both comparison studies did show that stationary mounted systems suffer from the not being able to track the sun as the day goes. The stationary systems then end up having very high angles of incidence. Both studies show clear decrease in absorbance and absorption of light throughout the days they were used, both in Tromsø and in Rome.

5.1 Further Work

How much the angle of incidence contribute to loss in solar cells and solar absorbers is still a question that is not fully answered. Even though the reflectance of the solar cells were found, the photon absorption was not determined so in order to do a full optical analysis for the solar cells, more parameters, like the quantum efficiency, need to be explored to draw a conclusion for them.

The polarized reflectance measurements show a clear decrease reflectance as the incident angle was shifted towards the polarization angle. A further study on the utilization of polarized light should be considered. What happens to the polarization as unpolarized light hit a reflective surface? How does the light polarize? It is possible to utilize the fact that the reflectance with p polarized light decreases as the angle of incident is shifted from near-perpendicular angles towards the polarization angle? The polarized results from the solar absorbers did also show results that did not coincide with the Fresnel equations, and is something that could be explored further.

Doing a full location comparison analysis to determine how much irradiance that hit the absorbing surface with similar monitoring censor data in Rome, as in Tromsø, would be interesting. With irradiance data from Rome, the latitudinal differences become much clearer. The investigation of the parameters that make a different outcome from the irradiance data needs to be further looked into, where the atmospheric path length is a very interesting factor.

A study that uses one- or two-axis tracking systems to follow the sun in the high latitudes, preferably to start off in Tromsø, to increase the amount of time of photon absorption and to compare losses and differences to the stationary systems.

A

Reflectance Results

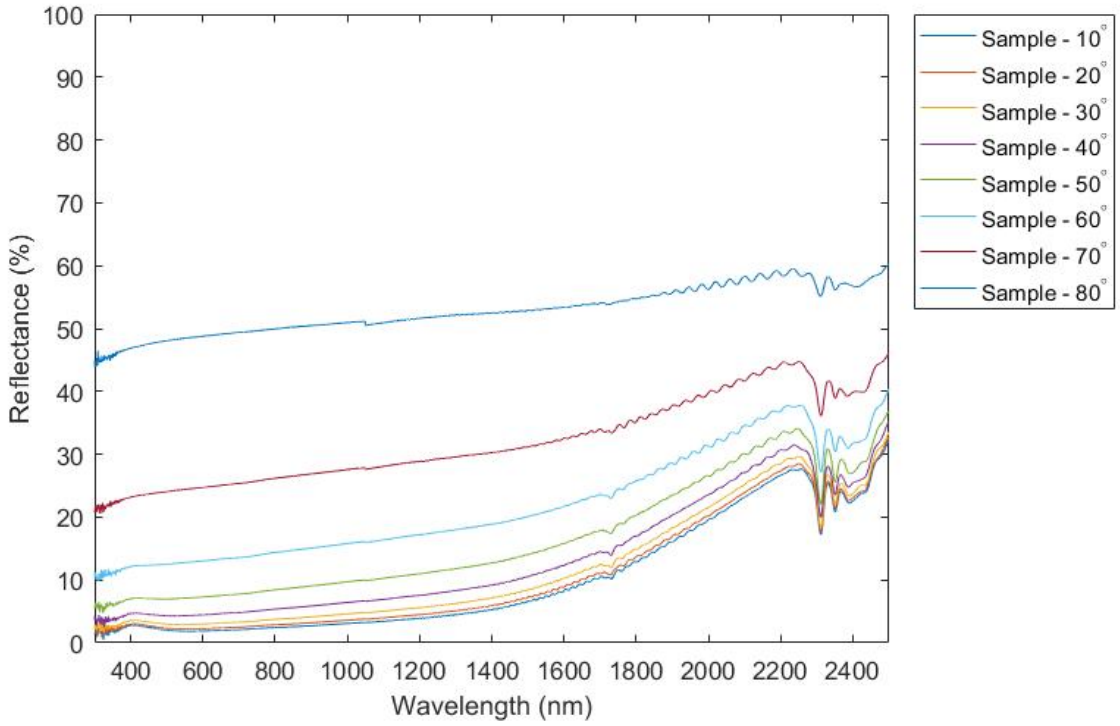

Figure A.1: Reflectance measurements of the Alanod sample for s polarized light.

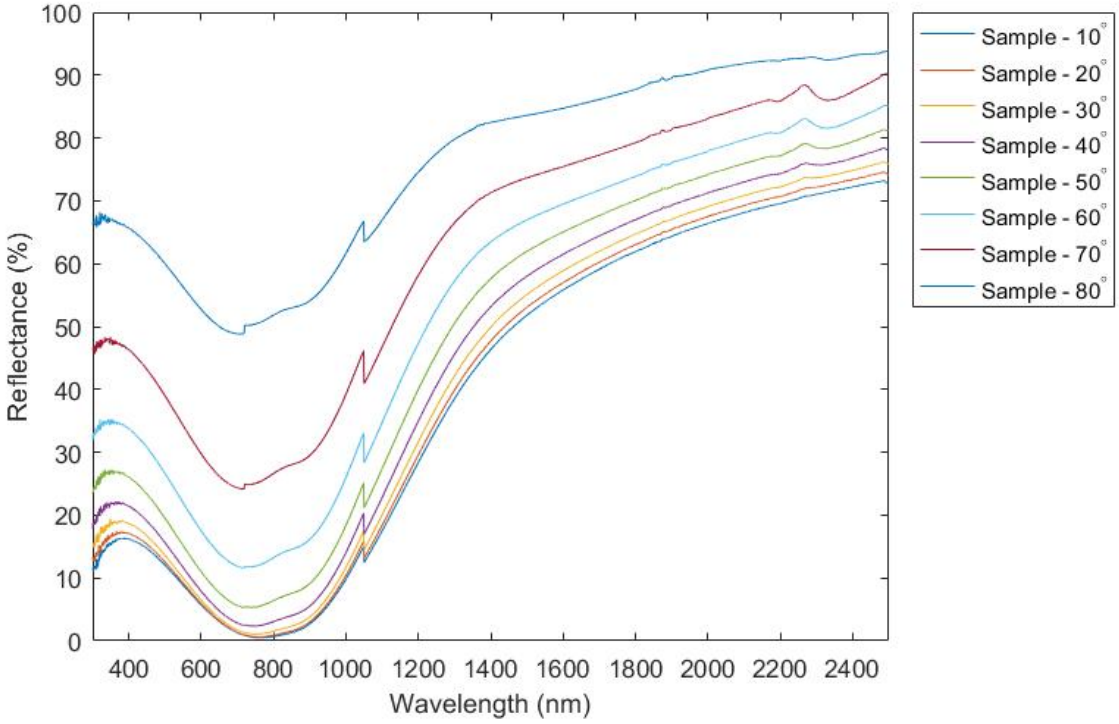

Figure A.2: Reflectance measurements of the SunStrip2 sample for s polarized light.

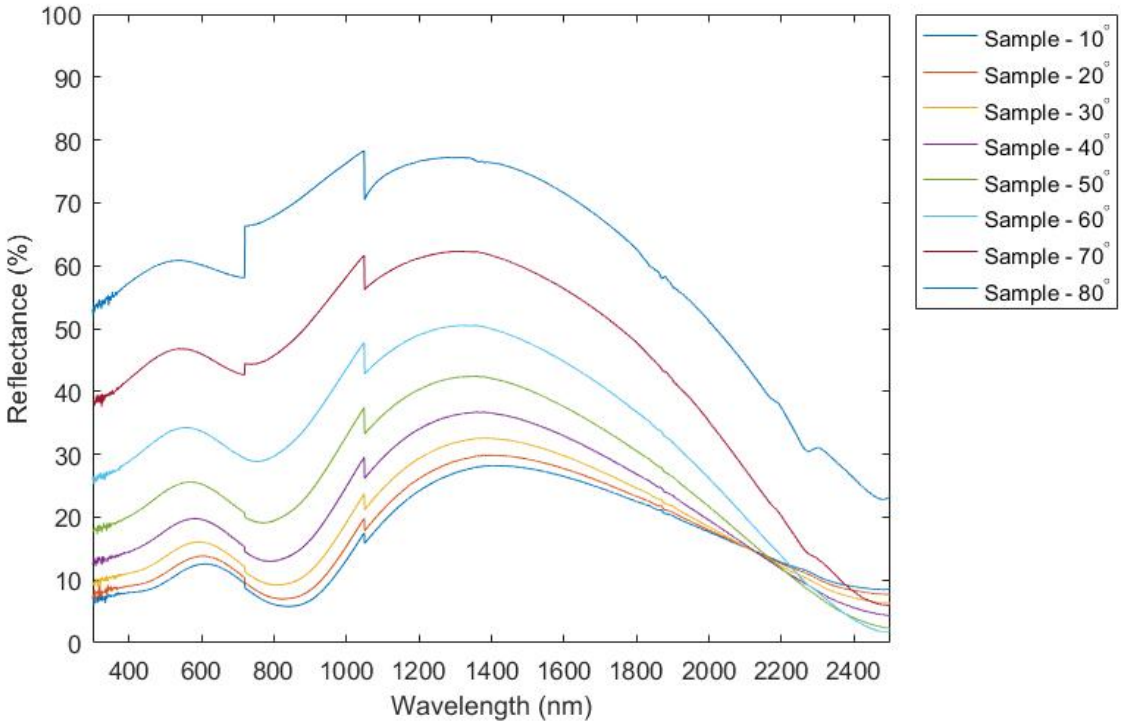

Figure A.3: Reflectance measurements of the SunStrip1 sample for s polarized light.

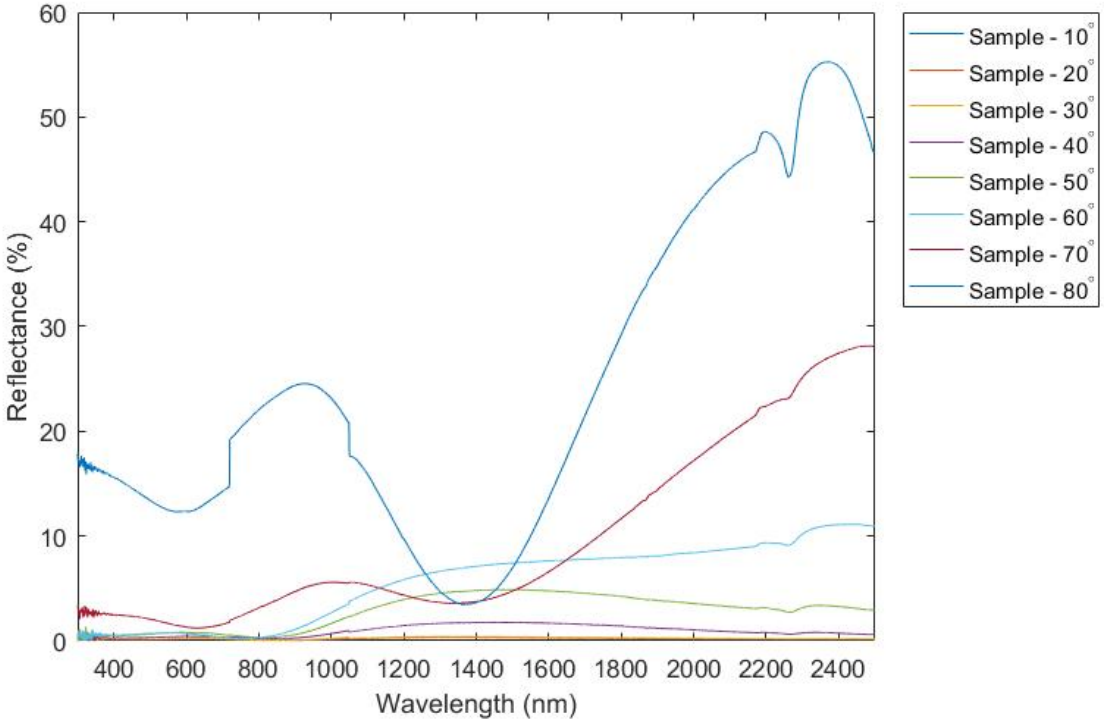

Figure A.4: Reflectance measurements of the SunStrip2 sample for p polarized light.

B

Matlab Code

B.1 Reflectance Plot

Listing B.1: Plotting of Reflectance Measurements

```
Q = csvread('cnt354-P-10-80.csv',2,2);
W10 = Q(:,1);
R10 = Q(:,2);
W20 = Q(:,3);
R20 = Q(:,4);
W30 = Q(:,5);
R30 = Q(:,6);
W40 = Q(:,7);
R40 = Q(:,8);
W50 = Q(:,9);
R50 = Q(:,10);
W60 = Q(:,11);
R60 = Q(:,12);
W70 = Q(:,13);
R70 = Q(:,14);
W80 = Q(:,15);
R80 = Q(:,16);

plot(W10,R10)
hold on
plot(W20,R20)
```

```
22 hold on
23 plot(W30,R30)
24 hold on
25 plot(W40,R40)
26 hold on
27 plot(W50,R50)
28 hold on
29 plot(W60,R60)
30 hold on
31 plot(W70,R70)
32 hold on
33 plot(W80,R80)
34 lgd = legend('Sample - 10^{\circ}','Sample - 20^{\circ}
       ','Sample - 30^{\circ}','Sample - 40^{\circ}','
       Sample - 50^{\circ}','Sample - 60^{\circ}','Sample -
        70^{\circ}','Sample - 75^{\circ}');
35 xlabel('Wavelength (nm)')
36 ylabel('Reflectance (%)')
37 set(lgd,'Location','northeastoutside')
38 set(gca,'Xlim',[300 2500])
39 set(gca,'Ylim',[0 50])
```

B.2 Calculation of Reflection Coefficient

Listing B.2: Calculation of Reflection Coefficients

```
n1 = 1;
n2 = 2.17;
phi = [10 20 30 40 50 60 70 80];

rrp = zeros(numel(phi),1);
for idx = 1:numel(phi)
    x = phi(idx);
    rp(x) = ((n1*sqrt(1-((n1/n2)*sind(x))^2) - n2*cosd(
       x))/(n1*sqrt(1-(1-(n1/n2)*sind(x))^2) + n2*cosd(
       x)))^2;
    rrp = rp;
end

rrs = zeros(1,numel(phi));
for idx = 1:numel(phi)
    x = phi(idx);
    rs(x) = ((n1*cosd(x) - n2*sqrt(1-((n1/n2)*sind(x))
       ^2))/(n1*cosd(x) + n2*sqrt(1-((n1/n2)*sind(x))
       ^2)))^2;
    rrs = rs;
end
```

B.3 Absorbance Calculation

This code was provided by my supervisor, Tobias Boström, and was originally made at Uppsala University. I have altered it to suit this thesis work.

Listing B.3: Absorbance Calculation with Reflectance measurements

```
clear;
figure;
%load UV-VIS-file
O = csvread('tobias-10-10-80.csv',2,16);
A=O;
A(:,2)=A(:,2)/100;      %Differs from lambdaftirmedsol

%load IR-fileA
load bk37.m;
AAA=bk37;
%prov='80/20% Si/HSi, 0.50M, 2000rpm, 50g/m->500,
    r031045, no IR';
prov='04513';
%prov='100/0, Si/SiH, 0.50M, 1500rpm, 50g/m->500,
    b031031, 031078';
%prov='50/50, Si/Ti, 0.43M, 4000rpm, 50g/m->500, b0379,
     03105';
%prov='70/30 Si/Ti, 0.48M, 50->500, 0397, 0.910 0.03,
    300h i kk test => k30';
%prov='ss2, 0.943 0.087, 300h i kk test => k32';
%prov='NiAl 65% 0.83M, 2750rpm, 50->550, 031058 new e
    meas';
%prov='70/30, Si/Ti, 0.48M, 2000rpm, 50g/m->500,
    b031014, t031015, not IR';
%prov='R cornig glass'

AAA=flipud(AAA);
%Reduce the number of datapoint
%with a factor 10 for 2-5 um
for i=1:1550
B(i)=AAA(i,2);
end
BB=decimate(B,10,4,'fir');
for i=1:155
AA(i,1)=AAA(10*i-5,1);
AA(i,2)=BB(i);
end
%with a factor 4 for 5-10 um
```

```
33 for i=1:524
34 C(i)=AAA(i+1550,2);
35 end
36 CC=decimate(C,4,4,'fir');
37 for i=1:131
38 AA(i+155,1)=AAA(1550+4*i-2,1);
39 AA(i+155,2)=CC(i);
40 end
41 %with a factor 2 for 10-20 um
42 for i= 1:258
43 D(i)=AAA(i+2075,2); %2074?
44 end
45 DD=decimate(D,2,4,'fir');
46 for i=1:129
47 AA(i+286,1)=AAA(2075+2*i,1); %borde vara?: AA(i+286,1)=
     AAA(2074+2*i-1,1)
48 AA(i+286,2)=DD(i);
49 end
50
51 %Transforming from cm-1 into um
52         AA(:,1)=10000./AA(:,1);
53
54 %Signal converted from 100% to 1 unit
55         AA(:,2)=AA(:,2)/100;
56
57 %Load file for the reflectance of the
     aluminiumreference.
58 load alref.m
59
60 % Interpolation of the  R-data of the
     aluminiumreference to the wavelengths of measured
     spectrum
61 Ra=interp1(alref(:,1),alref(:,2),AA(:,1));
62
63 %Correction for the reflectance of the alreference:
64 %AA(:,2)=Ra.*AA(:,2);
65 AA(:,2)=0.98*AA(:,2);
66
67 %
68 %Planck data for choosen temperature(now 373 K):
69 wa=AA(:,1)/1000000;
70 AE=AA(:,2);
71 %Extrapolation 20 - 100 um:
```

```
72 %the lenght should be 415!
73 m=length(wa);
74 for i=1:80
75 wa(m+i)=(20+i)*1e-6;
76 AE(m+i)=1-((20e-6^4)/wa(m+i)^4)*(1-(AA(411,2)+AA(412,2)
       +AA(413,2)+AA(414,2)+AA(415,2))/5);
77 end
78 pl=2*pi*6.62618e-34*(3e08^2);
79 planck(:,1)=pl./(wa.^5);
80 planck(:,1)=planck(:,1)./(exp((3e08*6.62618e-34)./(wa
       *373*1.3807e-23))-1);
81
82 % Here begins the numeric integration routine
83 %the lenght should be 415!
84 m=length(wa);
85 for i = 1:m-1
86          x(i)=wa(i+1)-wa(i);
87 end
88 for i = 1:m
89          s(i)=AE(i)*planck(i);
90 end
91 for i = 1:m-1
92          er(i)=(s(i)+s(i+1))*x(i)/2;
93          tot(i)=(planck(i)+planck(i+1))*x(i)/2;
94 end
95 ee=sum(er);
96 ee=1-ee/sum(tot)
97
98
99
100 % Loading the solarspectrum file (0.305<lambda<4.045 um
       )
101          load Sunspectrum.m;
102          Sun=Sunspectrum;
103 %Zero corrections if the zero file has nonzero values.
104 %        if A(1,3) > 0
105 %        A(:,3)=A(:,3)-0.003;
106 %        A(:,2)=A(:,2)-A(:,3);
107 %        A(:,4)=A(:,4)-A(:,3);
108 %        A(:,5)=A(:,5)-A(:,3);
109 %        end
110
```

```
111 % correcting the total reflectance ie case of B=0 and
        Fs=1:
112 %A(:,6)=0.98*A(:,4)./A(:,2);
113 %For lambda-nine:
114 A(:,6)=0.98*A(:,2);
115 % Sorting and transformation of the wavelength from nm
        into um
116         A(:,1)=A(:,1)/1000;
117         A=flipud(A);
118
119         n=length(Sun);
120         m=length(A);
121 % Gives condition wether an extrapolation should be
        performed or not and also
122 % calculates the extrapolated value (linear) by the
        least square method
123  if max(A(:,1)) <= max(Sun(:,1))
124
125 % Number of values that should be included in the
        extrapolation
126         p=3;
127
128         for i = 1:p
129                 d(i)=A(m+1-i,1);
130                 e(i)=(d(i))^2;
131                 f(i)=A(m+1-i,2);
132                 g(i)=A(m+1-i,1)*A(m+1-i,4);
133         end
134
135         a=(p*sum(g)-sum(d)*sum(f))/(p*sum(e)-(sum(d))
                ^2);
136         b=(sum(f)-a*sum(d))/p;
137
138         A(m+1,1)=4.1;
139         A(m+1,6)=a*A(m+1,1)+b;
140
141 % If the extrapolated value exceedes 1 or falls bellow
        0 the value is set to 1 or 0
142         if A(m+1,6) >= 1
143                 A(m+1,6)=1;
144         elseif A(m+1,6) <= 0
145                 A(m+1,6)=0;
146         end
```

```
147 end
148 % Interpolation of the measured R to the wavelengths of
        sun's spectrum
149 y=interp1(A(:,1),A(:,6),Sun(:,1));
150
151 % Here begins the numeric integration routine
152 for i = 1:n-1
153         x(i)=Sun(i+1,1)-Sun(i,1);
154 end
155 for i = 1:n
156         s(i)=y(i)*Sun(i,2);
157 end
158 for i = 1:n-1
159         ar(i)=(s(i)+s(i+1))*x(i)/2;
160 end
161 a=1-sum(ar)/767.2
162 %Preparing for a plot of total corrected data:
163 for i=1:m
164 R(i,1)=A(i,1);
165 R(i,2)=A(i,6);
166 end
167 n=length(AE);
168 for i=1:n-51
169 %R(i+m,1)=AA(i+51,1);
170 %R(i+m,2)=AA(i+51,2);
171 R(i+m,1)=wa(i+51)*1e6;
172 R(i+m,2)=AE(i+51);
173 end
174
175 r=length(R(:,1))
176 s=length(Sun)
177
178 d=max(Sun(:,2))
179 for i = 1:length(Sun)
180         S(i)=Sun(i,2)/d;
181 end
182 l=length(S)
183 % Plot settings
184 h=plot(R(:,1),R(:,2));
185 hold on;
186 plot(Sun(:,1),S);
187 set(h,'color','r');
188 %set(gcf,'defaulttextcolor','black')
```

```
189 %set(gcf,'color','w');
190 %set(gca,'xcolor','b');
191 %set(gca,'ycolor','b');
192  set(gca,'xlim',[0.3 20]);
193  set(gca,'xscale','log');
194  set(gca,'xtick',[1.0 10 20]);
195  set(gca,'ylim',[0 1.0]);
196  title(['a:',num2str(a),' e:',num2str(ee), '  #',num2str
       (prov)]);
197  xlabel('wavelength (um)');
198  ylabel('Reflectance');
199  grid;
200  save test.dat /ascii R;
```

B.4 Absorbance Plot

Listing B.4: Absorbance and Incident Angle as a function of Time of Day

```
% Angle-Dependent Absorption Data from Measurements
y1 = [0.9668 0.9646 0.9601 0.9513 0.9336 0.8947 0.8017
    0.5803];
x1 = [10 20 30 40 50 60 70 80];

% Regression - Polynomial Fit
ada = polyfit(x1,y1,5);
x2 = linspace(10,80);
adafit = polyval(ada,x2);

% Quantification/Comparison

% Aquiring angle and time data.
% Arrays for time and angles
% tt - TimeTromso, at - AngleTromo, tr - TimeRome, ar -
    AngleRome

% Tromso 15.april
tt15apr = 24*xlsread('comparison.xlsx', 'A4:A66');
at15apr = xlsread('comparison.xlsx', 'B4:B66');

% Tromso 15.june
tt15jun = 24*xlsread('comparison.xlsx', 'C27:C87');
at15jun = xlsread('comparison.xlsx', 'D27:D87');

% Tromso 15.september
tt15sep = 24*xlsread('comparison.xlsx', 'E4:E57');
at15sep = xlsread('comparison.xlsx', 'F4:F57');

% Rome 15. april
tr15apr = 24*xlsread('comparison.xlsx', 'G4:G56');
ar15apr = xlsread('comparison.xlsx', 'H4:H56');

% Rome 15. june
tr15jun = 24*xlsread('comparison.xlsx', 'I4:I64');
ar15jun = xlsread('comparison.xlsx', 'J4:J64');

% Rome 15. september
tr15sep = 24*xlsread('comparison.xlsx', 'K4:K53');
ar15sep = xlsread('comparison.xlsx', 'L4:L53');

```

```
40 % Adjusting incident angle with respect to surface
       normal of Solar Module
41 % Tromso
42 incangt = 90 - (40 + at15jun);
43 iangabst = abs(incangt);
44 iangabsreft = iangabst;
45
46 % Loop for Calculating the Angle-Dependent Absorption
       from Regression in
47 % Tromso
48 AAT = zeros(1,numel(iangabsreft));
49 for idx = 1:numel(iangabsreft)
50     A = iangabsreft(idx);
51     alfa = -0.000000001077244*A^5 +0.000000173014277*A
           ^4 - ...
52     0.000011107852564*A^3 +0.000325329108392*A^2 -
           0.004501303613053*A + 0.988825000000002;
53     AAT(idx) = alfa;
54 end
55
56 % Rome
57 incangr = 90 - (40 + ar15jun);
58 iangabsr = abs(incangr);
59 iangabsrefr = iangabsr;
60
61 % Loop for Calculating the Angle-Dependent Absorption
       from Regression in
62 % Rome
63 AAR = zeros(1,numel(iangabsrefr));
64 for idx = 1:numel(iangabsrefr)
65     A = iangabsrefr(idx);
66     alfa = -0.000000001077244*A^5 +0.000000173014277*A
           ^4 - ...
67     0.000011107852564*A^3 +0.000325329108392*A^2 -
           0.004501303613053*A + 0.988825000000002;
68     AAR(idx) = alfa;
69 end
70
71 % Plot - Regression and Measured Data
72 % plot(x1,y1,'*')
73 % hold on
74 % plot(x2,adafit)
75 % hold on
```

```
% lgd = legend('Calculated Absorption','Regression
    Analysis');
% set(lgd, 'Location', 'southeast')
% xlabel('Incident Angle of Light(\circ)')
% ylabel('Absorbance')
% set(gca,'Ylim',[0 1])
% set(gca,'Xlim',[10 80])

% Average Absorbance throughout the day
MT = mean(AAT);
MR = mean(AAR);

 % Plot - Absorbance and Angle vs. Time of day
 yyaxis left
 plot(tt15jun, AAT);
 hold on
 plot(tr15jun, AAR);
 hold on
 xlabel('Time of Day(h)')
 ylabel('Absorbance')
 set(gca, 'Ylim', [0 1])
 yyaxis right
 plot(tt15jun, iangabsreft);
 hold on
 plot(tr15jun, iangabsrefr);
 hold on
 ylabel('Angle({\circ})')
 lgd = legend('Absorbance - Tromso', 'Absorbance - Rome
    ', 'Incident Angle of Sun - Tromso', 'Incident
    Angle of Sun - Rome');
 set(lgd,'Location', 'northeastoutside');
 %datetick('x','HHMM')
 set(gca,'Xlim',[0 24])
 set(gca,'Ylim',[0 100])
```

B.5 Angle-Dependent Absorbance Plot with Solar Edge Irradiance Data

Listing B.5: Angle-Dependent Absorbance Plot with Solar Edge Irradiance Data

```
% Parameters for checking the angle-dependent impact in reality
tt17apr = 24*xlsread('realitycheck.xlsx', 'A4:A68'); % Time
SolEdge = xlsread('realitycheck.xlsx', 'B4:B68'); % W/m^2
at17apr = xlsread('realitycheck.xlsx', 'C4:C68'); % Elevation Angle

% Adjusting incident angle with respect to surface normal of Solar Module
% Tromso
incangtr = 90 - (40 + at17apr);
iangabstr = abs(incangtr);

% Setting parameters to calculate the Angle of Incidence
d = 107;                                % Day of the year (17th of april)
dd = -23.45*cosd((360/365)*(d+10)); % Inclination Angle
p = 69;                                 % Latitude angle Tromso
b = 40;                                 % 90-tilt to surface(40 deg)
a = at17apr;


% Calculating the Hour Angle
alpha = zeros(1, numel(a));
for i = 1:numel(a)
    aa = a(i);
    w = asind((sind(aa) - sind(d)*sind(p))/sind(p));
    alpha(i) = w;
end

% Calculating Angle of Incidence
theta = zeros(1,numel(alpha));
for y = 1:numel(alpha)
    yy = alpha(y);
```

```
31      ti = acosd(cosd(dd)*cosd(p-b)*cosd(yy) + sind(dd)*
            sind(p-b));
32      theta(y) = ti;
33  end
34
35  AAA = zeros(numel(theta),1);
36  for idx = 1:numel(theta)
37      A = theta(idx);
38      alfaa = -0.000000001077244*A^5 +0.000000173014277*A
            ^4 - ...
39      0.000011107852564*A^3 +0.000325329108392*A^2 -
            0.004501303613053*A + 0.988825000000002;
40      AAA(idx) = alfaa;
41  end
42
43  n = SolEdge.*AAA;
44  diff = SolEdge-n;
45  averagediff = mean(diff);
46
47  figure(1)
48  plot(tt17apr,SolEdge,'r')
49  hold on
50  plot(tt17apr,n,'Color',[.0 .5 .0])
51  xlabel('Time of Day(h)')
52  ylabel('Irradiance(W/m^2)')
53  lgd = legend('Direct Irradiance','Absorbed Irradiance')
        ;
54  set(lgd,'Location','northeastoutside')
55
56  figure(2)
57  yyaxis right
58  plot(tt17apr,theta,'r')
59  hold on
60  set(gca,'Ylim', [0 100])
61  ylabel('Incident Angle(\circ)')
62  xlabel('Time of Day(h)')
63
64
65  yyaxis left
66  plot(tt17apr,AAA,'b')
67  ylabel('Absorbance')
68  set(gca,'Ylim', [0 1])
69  lgd = legend('Angle Dependent Absorbance','Angle of
```

```
    Incidence(\circ)');
70 set(lgd,'Location','northeastoutside')
71
72
73 figure(3)
74 plot(tt17apr, diff,'r');
75 hold on
76 plot(tt17apr, ones(size(tt17apr))*averagediff,'Color'
    ,[.0 .5 .0])
77 xlabel('Time of Day(h)')
78 ylabel('Irradiance(W/m^2)')
79 lgd = legend('Difference between Direct and Absorbed','
    Averaged Difference');
80 set(lgd,'Location','northeastoutside')
```

Bibliography

Alternative Energy Tutorials. (2018). *http://www.alternative-energy-tutorials.com*. Retrieved from http://www.alternative-energy-tutorials.com/solar-hot-water/evacuated-tube-collector.html

Asadollahbaik, A., Boden, S. A., Charlton, M. D., Payne, D. N., Cox, S., & Bagnall, D. M. (2014). Reflectance properties of silicon moth-eyes in response to variations in angle of incidence, polarisation and azimuth orientation. *Optics express*, *22*(102), A402–A415.

Bermel, P., Lee, J., Joannopoulos, J. D., Celanovic, I., & Soljacie, M. (2012). Selective solar absorbers. *Annual Review of Heat Transfer*, *15*(15), 231–254.

Boström, T. (2006). *Solution-chemically derived spectrally selective solar absorbers: with system perspectives on solar heating* (Unpublished doctoral dissertation). Acta Universitatis Upsaliensis.

Casio Computer. (2018). *http://www.keisan.casio.com*. Retrieved from https://keisan.casio.com/exec/system/1224682277

Chan, C., Hallam, B., & Wenham, S. (2012). Simplified interdigitated back contact solar cells. *Energy Procedia*, *27*, 543–548.

Chapin, D. M., Fuller, C., & Pearson, G. (1954). A new silicon p-n junction photocell for converting solar radiation into electrical power. *Journal of Applied Physics*, *25*(5), 676–677.

Chen, Z. (2016). Carbon nanotube spectrally selective solar thermal absorbers.

Du, C.-H., Wang, T.-Y., Chen, C.-H., & Yeh, J. A. (2014). Fabrication of an ultra-thin silicon solar cell and nano-scale honeycomb structure by thermal-stress-induced pattern transfer method. *Thin Solid Films*, *557*, 372–375.

EFCsolar. (2016). *http://www.efcsolar.com/*. Retrieved from http://www.efcsolar.com/solar-systems

Fundamentals of Environmental Measurements. (2016). *www.fondriest.com*.

Retrieved from https://www.fondriest.com/environmental-measurements/parameters/weather/photosynthetically-active-radiation/

Hua, X.-S., Zhang, Y.-J., & Wang, H.-W. (2010). The effect of texture unit shape on silicon surface on the absorption properties. *Solar Energy Materials and Solar Cells*, *94*(2), 258–262.

Ingenito, A., Isabella, O., & Zeman, M. (2015). Nano-cones on micro-pyramids: modulated surface textures for maximal spectral response and high-efficiency solar cells. *Progress in Photovoltaics: Research and Applications*, *23*(11), 1649–1659.

ISC Konstanz. (2018). *Home page of isc konstanz.* Retrieved from http://isc-konstanz.de/

Jansen, H., De Boer, M., Wensink, H., Kloeck, B., & Elwenspoek, M. (2001). The black silicon method. viii. a study of the performance of etching silicon using sf6/o2-based chemistry with cryogenical wafer cooling and a high density icp source. *Microelectronics Journal*, *32*(9), 769–777.

Jäger-Waldau, A. (2016). *Pv status report 2016* (Vol. EUR 28159 EN) (No. doi:10.2790/749737).

Kempe, M. D. (2010). Ultraviolet light test and evaluation methods for encapsulants of photovoltaic modules. *Solar Energy Materials and Solar Cells*, *94*(2), 246–253.

Kempe, M. D., Jorgensen, G. J., Terwilliger, K. M., McMahon, T. J., Kennedy, C. E., & Borek, T. T. (2007). Acetic acid production and glass transition concerns with ethylene-vinyl acetate used in photovoltaic devices. *Solar Energy Materials and Solar Cells*, *91*(4), 315–329.

McIntosh, K. R., Cotsell, J. N., Cumpston, J. S., Norris, A. W., Powell, N. E., & Ketola, B. M. (2009). An optical comparison of silicone and eva encapsulants for conventional silicon pv modules: A ray-tracing study. In *Photovoltaic specialists conference (pvsc), 2009 34th ieee* (pp. 000544–000549).

Moreno, M., Daineka, D., & i Cabarrocas, P. R. (2010). Plasma texturing for silicon solar cells: From pyramids to inverted pyramids-like structures. *Solar Energy Materials and Solar Cells*, *94*(5), 733–737.

Moreno, M., Murias, D., Martínez, J., Reyes-Betanzo, C., Torres, A., Ambrosio, R., . . . Escobar, M. (2014). A comparative study of wet and dry texturing processes of c-si wafers for the fabrication of solar cells. *Solar Energy*, *101*,

182–191.

Pillai, S., Catchpole, K., Trupke, T., & Green, M. (2007). Surface plasmon enhanced silicon solar cells. *Journal of applied physics*, *101*(9), 093105.

PVEducation. (2018). *http://www.pveducation.org*. Retrieved from `http://www.pveducation.org/pvcdrom/properties-of-sunlight/air-mass`

Singh, P. K., Kumar, R., Lal, M., Singh, S., & Das, B. (2001). Effectiveness of anisotropic etching of silicon in aqueous alkaline solutions. *Solar Energy Materials and Solar Cells*, *70*(1), 103–113.

Solanki, C. S. (2015a). *Solar photovoltaics: Fundamentals, technologies and applications, third edition*. Rimijhim House, 111, Patparganj Industrial Estate, Delhi- 110092: Asoke K. Ghosh, PHI Learning Private Limited.

Solanki, C. S. (2015b). *Solar photovoltaics: Fundamentals, technologies and applications, third edition*. Rimijhim House, 111, Patparganj Industrial Estate, Delhi- 110092: Asoke K. Ghosh, PHI Learning Private Limited.

Solar Edge. (2018). *Monitoring page of solar edge.* Retrieved from `https://www.solaredge.com/us/products/pv-monitoring#/`

Steam of Boiler. (2018). *http://steamofboiler.blogspot.no/*. Retrieved from `http://steamofboiler.blogspot.no/2011/08/flat-plate-solar-collector.html`

Willeke, G., Nussbaumer, H., Bender, H., & Bucher, E. (1992). A simple and effective light trapping technique for polycrystalline silicon solar cells. *Solar Energy Materials and Solar Cells*, *26*(4), 345–356.

Wood, R. (1902). Xliv. a suspected case of the electrical resonance of minute metal particles for light-waves. a new type of absorption. *The London, Edinburgh, and Dublin Philosophical Magazine and Journal of Science*, *3*(16), 396–410.

Yoo, J. (2010). Reactive ion etching (rie) technique for application in crystalline silicon solar cells. *Solar Energy*, *84*(4), 730–734.